


ORIGINAL RESEARCH

Proteolytic Degradation Is a Major Contributor to Bioprosthetic Heart Valve Failure

Alexander E. Kostyunin , PhD; Tatiana V. Glushkova, PhD; Arseniy A. Lobov , PhD; Evgeny A. Ovcharenko, PhD; Bozhana R. Zainullina , MSc; Leo A. Bogdanov , MSc; Daria K. Shishkova, PhD; Victoria E. Markova , MSc; Maksim A. Asanov , MSc; Rinat A. Mukhamadiyarov , PhD; Elena A. Velikanova , PhD; Tatiana N. Akentyeva , MSc; Maria A. Rezvova , MSc; Alexander N. Stasev , MD, PhD; Alexey V. Evtushenko, MD, DSc; Leonid S. Barbarash, MD, DSc; Anton G. Kutikhin , MD, PhD

BACKGROUND: Whereas the risk factors for structural valve degeneration (SVD) of glutaraldehyde-treated bioprosthetic heart valves (BHVs) are well studied, those responsible for the failure of BHVs fixed with alternative next-generation chemicals remain largely unknown. This study aimed to investigate the reasons behind the development of SVD in ethylene glycol diglycidyl ether-treated BHVs.

METHODS AND RESULTS: Ten ethylene glycol diglycidyl ether-treated BHVs excised because of SVD, and 5 calcified aortic valves (AVs) replaced with BHVs because of calcific AV disease were collected and their proteomic profile was deciphered. Then, BHVs and AVs were interrogated for immune cell infiltration, microbial contamination, distribution of matrix-degrading enzymes and their tissue inhibitors, lipid deposition, and calcification. In contrast with dysfunctional AVs, failing BHVs suffered from complement-driven neutrophil invasion, excessive proteolysis, unwanted coagulation, and lipid deposition. Neutrophil infiltration was triggered by an asymptomatic bacterial colonization of the prosthetic tissue. Neutrophil elastase, myeloblastin/proteinase 3, cathepsin G, and matrix metalloproteinases (MMPs; neutrophil-derived MMP-8 and plasma-derived MMP-9), were significantly overexpressed, while tissue inhibitors of metalloproteinases 1/2 were downregulated in the BHVs as compared with AVs, together indicative of unbalanced proteolysis in the failing BHVs. As opposed to other proteases, MMP-9 was mostly expressed in the disorganized prosthetic extracellular matrix, suggesting plasma-derived proteases as the primary culprit of SVD in ethylene glycol diglycidyl ether-treated BHVs. Hence, hemodynamic stress and progressive accumulation of proteases led to the extracellular matrix degeneration and dystrophic calcification, ultimately resulting in SVD.

CONCLUSIONS: Neutrophil- and plasma-derived proteases are responsible for the loss of BHV mechanical competence and need to be thwarted to prevent SVD.

Key Words: bacterial invasion ■ bioprosthetic heart valves ■ matrix metalloproteinases ■ neutrophil infiltration ■ structural valve degeneration

Replacement by mechanical or bioprosthetic heart valves (BHVs) remains the mainstay of heart valve disease treatment,^{1,2} with >200 000 interventions annually worldwide and a predicted number of 850 000 by 2050.^{3,4} In contrast with mechanical heart valves,

BHVs have the advantage of high hemocompatibility and do not demand lifelong use of anticoagulants.⁵ However, BHVs are not capable of regeneration as their biomaterial (eg, bovine or porcine pericardium) mandatorily undergoes chemical fixation, and therefore the life

Correspondence to: Anton G. Kutikhin, MD, PhD, Laboratory of Molecular, Translational, and Digital Medicine, Research Institute for Complex Issues of Cardiovascular Diseases, 6 Sosnovy Boulevard, Kemerovo 650002, Russian Federation. Email: antonkutikhin@gmail.com

Supplemental Material is available at <https://www.ahajournals.org/doi/suppl/10.1161/JAHA.122.028215>

For Sources of Funding and Disclosures, see page 16.

© 2022 The Authors. Published on behalf of the American Heart Association, Inc., by Wiley. This is an open access article under the terms of the [Creative Commons Attribution-NonCommercial](#) License, which permits use, distribution and reproduction in any medium, provided the original work is properly cited and is not used for commercial purposes.

JAHA is available at: www.ahajournals.org/journal/jaha

CLINICAL PERSPECTIVE

What Is New?

- Here, we for the first time performed a comparative proteomic profiling of distinct bioprosthetic heart valves and calcified aortic valves, having found that structural valve degeneration and calcific aortic valve disease are vastly different conditions, and structural valve degeneration is notable for the complement-mediated neutrophil attack of the prosthetic tissue, which commonly suffers from asymptomatic bacterial colonization.
- Further, we identified a number of neutrophil-secreted (neutrophil elastase, myeloblastin/proteinase [PRTN3], matrix metalloproteinase-8, and cathepsin G) and plasma-derived (matrix metalloproteinase-9) proteases, which are unique or overrepresented in the bioprosthetic heart valves as compared with the calcified aortic valves.
- In contrast to other proteases, matrix metalloproteinase-9 was ubiquitously expressed, being primarily colocalized with the degraded extracellular matrix and therefore representing the primary culprit of structural valve degeneration, although neutrophil-derived proteases also made a significant contribution.

What Are the Clinical Implications?

- As proteolytic degradation is responsible for the failure of calcification-protected bioprosthetic heart valves, we suggest the development of the protective sheath blocking the proteases and repulsing bacteria and immune cells as a promising strategy to create a structural valve degeneration- and calcification-resistant, lifelong-implantable bioprosthetic heart valve.

Nonstandard Abbreviations and Acronyms

AV	aortic valve
BHV	bioprosthetic heart valve
CAVD	calcific aortic valve disease
ECM	extracellular matrix
EGDE	ethylene glycol diglycidyl ether
MMP	matrix metalloproteinase
NE/ELA2	neutrophil elastase
PRTN3	myeloblastin/proteinase 3
SVD	structural valve degeneration
TIMP	tissue inhibitor of metalloproteinases
XAP-BHVs	xenoaortic porcine bioprosthetic heart valves
XPB-BHVs	xenopericardial bovine bioprosthetic heart valves

span of these prostheses is significantly limited by structural valve degeneration (SVD).^{6,7} SVD is defined as an irreversible degeneration of BHVs upon the implantation and is accompanied by the delamination, fragmentation, perforation, tearing, and calcification of the prosthetic leaflets.^{6,7} These structural defects eventually lead to the mechanical incompetence of the BHVs, culminating in a hemodynamic insufficiency.^{6,7} According to the expert estimates, almost one-third of the BHVs require replacement within 15 years after implantation because of SVD, and this problem is far from its resolution.^{8,9}

Hitherto, the majority of implanted BHVs have been pretreated with glutaraldehyde to prevent enzymatic degradation and reduce immunogenicity by protein cross linking.¹⁰ Nevertheless, such fixation regimen does not protect the prosthetic tissue from calcification, as the negative surface charge of aldehyde groups attracts positively charged Ca²⁺ ions from the blood, leading to their accumulation in the degraded extracellular matrix (ECM).^{10,11} Next-generation chemical fixation regimens include ethylene glycol diglycidyl ether (EGDE), and EGDE-treated BHVs have demonstrated acceptable long-term results even in young patients (~45 years of age) who generally exhibit accelerated calcification.^{12,13} Further, EGDE-treated BHVs showed better performance in a pulmonary position upon 8 to 10 years of follow-up, as compared with glutaraldehyde-treated BHVs.^{14,15} Still, EGDE-treated BHVs are not fully protected from SVD. The causes of SVD in EGDE-treated BHVs have not been investigated so far.

Despite significant differences in triggers of calcific aortic valve disease (CAVD), that is, endothelial dysfunction, lipid deposition, intravalvular hemorrhage, myofibroblastic and osteochondrogenic differentiation of valvular interstitial cells, and SVD (residual immunogenicity of the prosthetic biomaterial, inability to synthesize and repair the ECM components, gradual disintegration of prosthetic tissue under the cyclic load, and dystrophic calcification), both native aortic valves (AVs) and BHVs suffer from the macrophage infiltration, ECM degradation, and ectopic mineralization (although the mechanisms of the latter are different in the AVs and BHVs, as indicated above).^{16–20}

Here, we for the first time performed a comparative proteomic profiling of BHVs (having either bovine or porcine origin) and calcified AVs excised because of SVD and CAVD, respectively. We identified 5 major protein categories overrepresented in BHV: complement components, neutrophil-associated proteins, matrix proteases, coagulation-specific proteins, and lipid-associated proteins. Overexpressed together, complement components and neutrophil markers suggested a microbial colonization of the BHVs upon the implantation that was confirmed by the Gram staining and polymerase chain reaction, although blood

inoculation was negative and the patients had no clinical or echocardiographic signs of infective endocarditis. Collectively, proteomic profiling and dot blotting screening found plasma- and neutrophil-derived proteases considerably upregulated and tissue inhibitors of metalloproteinases downregulated in the BHVs in comparison with calcified AVs, indicating uncontrolled proteolysis within the former. Differential immunostaining showed that matrix metalloproteinase (MMP) 9 has been primarily colocalized with the degraded ECM, indicating the plasma as the main source of this proteolytic enzyme, while neutrophil elastase (NE/ELA2) and MMP-8 were specific for immune cells and were abundantly expressed in numerous neutrophils invading the BHVs. To summarize, we suggest that plasma- and neutrophil-derived proteases are responsible for the loss of BHV mechanical competence.

METHODS

Here, we interrogated 11 EGDE-treated BHVs (KemCor, PeriCor or UniLine, NeoCor) removed during the repeated heart valve replacement because of their failure, as well as 5 AVs excised during the primary heart valve replacement because of CAVD. The timing of the excision was defined according to the 2020 American College of Cardiology/American Heart Association guideline for the management of patients with valvular heart disease.¹ AVs have been excised because of severe and symptomatic calcific aortic stenosis diagnosed at transthoracic echocardiography (stages D1–D3, where stage D1 was defined as maximum velocity ≥ 4 m/s or mean systolic pressure gradient between the left ventricle and aorta ≥ 40 mmHg; stage D2 was defined as < 4 m/s, aortic valve area ≤ 1.0 cm², left ventricular ejection fraction $< 50\%$, and maximum velocity at dobutamine stress echocardiography ≥ 4 m/s at any flow rate; and stage D3 was defined as maximum velocity < 4 m/s, aortic valve area ≤ 1.0 cm², aortic valve area index ≤ 0.6 cm²/m², and stroke volume index < 35 mL/m²). In turn, BHVs have been excised because of severe stenosis or regurgitation defined as stage 3 SVD according to the Valve Academic Research Consortium criteria published in 2018.⁷ KemCor and PeriCor are xenoaortic (porcine) BHVs (XAP-BHVs, $n=5$) while UniLine is a xenopericardial (bovine) BHV (XPB-BHVs, $n=6$). Sample collection and preparation are described in [Figure S1](#). The investigation was carried out in accordance with the Good Clinical Practice and the Declaration of Helsinki. The study protocol was approved by the Local Ethical Committee of Research Institute for Complex Issues of Cardiovascular Diseases (Protocol No. 20190606, date of approval: June 6, 2019). All patients provided written informed consent after receiving a full explanation of

the study. Criteria of inclusion were (1) replacement of EGDE-treated BHV because of its failure (or replacement of the AV because of CAVD), (2) absence of any clinical and echocardiographic signs of infective endocarditis as well as negative blood inoculation before the surgery according to the respective European Society of Cardiology guidelines,²¹ and (3) signed written informed consent to participate in the study. Criteria of exclusion were (1) any gross signs of prosthetic valve endocarditis or any positive blood inoculation upon the BHV or AV replacement, and (2) withdrawal of the written informed consent to participate in the study. Sex distribution and prevalence of comorbid conditions did not differ significantly between the recipients of XAP-BHVs and recipients of XPB-BHVs ([Table S1](#)). Clinico- and histopathological features of the BHV types and calcified AVs are documented in [Table S2](#) and [S3](#).

The authors declare that all supporting data are available within the article and its Online Data Supplement containing Data [S1](#).

RESULTS

Bioprosthetic Heart Valves Are Enriched With Complement Components, Neutrophils, Matrix Metalloproteinases, Platelet/Coagulation Markers, and Lipid-Associated Proteins

To conduct an unbiased analysis of the proteins enriched in failing BHVs and calcified AVs, we performed a shotgun proteomic profiling by means of ultra-high-performance liquid chromatography–tandem mass spectrometry with ion mobility in parallel accumulation–serial fragmentation mode (timsToF Pro, ultra-high-performance liquid chromatography–tandem mass spectrometry). Partial least squares discriminant analysis has shown that XAP-BHVs and XPB-BHVs are notably different from calcified AVs while being similar to each other in terms of human protein composition ([Figure 1A](#)). Bioinformatic analysis found as few as 2 differentially expressed human proteins between XAP-BHVs and XPB-BHVs, as evident by volcano plot ([Figure 1B](#)). Of 1614 proteins identified, 73 were unique for BHVs, and 70 were overexpressed in the BHVs. Of these 143 proteins, 75 belonged to 5 major categories: complement components,¹⁹ neutrophil markers,¹⁹ matrix proteases,⁷ platelet markers and coagulation factors,¹⁸ and proteins involved into the lipid metabolism¹² ([Figure 2](#)). Strikingly, BHVs overexpressed 8 of 8 components of the membrane attack complex (CO5/6/7/8A/8B/8G/9 and clusterin) along with the neutrophil-specific antimicrobial proteins (myeloperoxidase, nicotinamide adenine dinucleotide phosphate hydrogen oxidase 2, neutrophil cytosolic

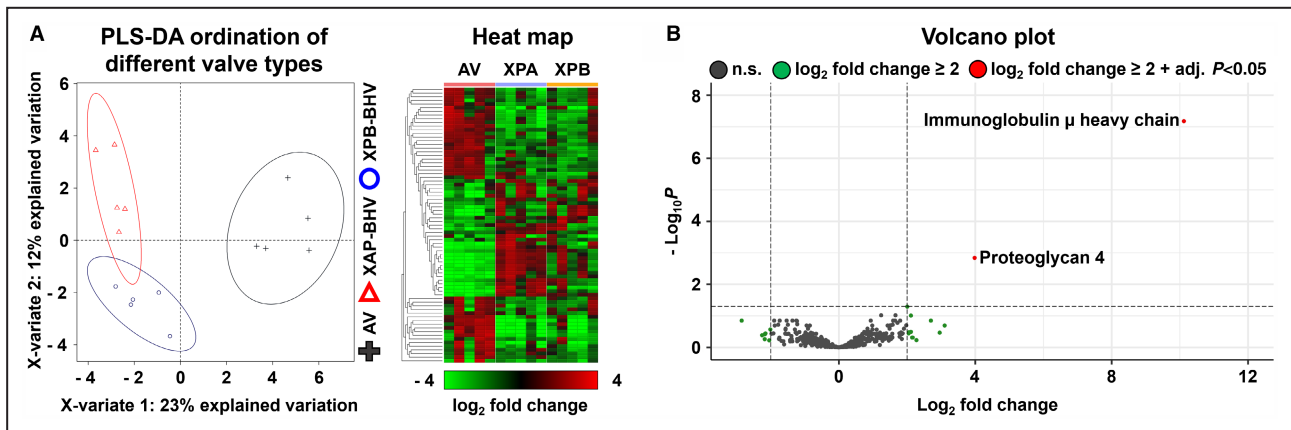


Figure 1. Label-free proteomic profiling of calcified AVs, XAP-BHVs, and XPB-BHVs.

A, PLS-DA and heat map demonstrated considerable differences between the AVs and BHVs, while XAP-BHVs and XPB-BHVs have not been significantly different from each other with regards to the proteomic composition. **B**, Volcano plot illustrates the absence of statistically significant differences between XAP-BHVs and XPB-BHVs, showing only 2 different proteins. AVs indicates aortic valves; PLS-DA, partial least squares discriminant analysis; XAP-BHVs, xenoaortic porcine bioprosthetic heart valves; and XPB-BHVs, xenopericardial bovine bioprosthetic heart valves.

factor 1, Ras-related C3 botulinum toxin substrate 2, cathelicidin, eosinophil cationic protein, S100A8/9, neutrophil defensin 1, lactotransferrin) and neutrophil-derived proteases (ELNE/ELA2, PRTN3, cathepsin G, MMP-8/9) while tissue inhibitors of metalloproteinases (TIMP-1/2) were downregulated as compared with the calcified AVs (Figure 2). Taken together, these findings strongly suggested that SVD is markedly different from CAVD with regard to the proteomic signatures of complement attack, neutrophil invasion, and ECM remodeling.

Bioprosthetic Heart Valves Suffer From the Neutrophil Infiltration Triggered By an Asymptomatic Bacterial Colonization

With the aim to investigate the immune cell profile of BHVs and AVs, we performed an electron microscopy analysis using the original embedding and backscattered scanning electron microscopy method,²² which allows ultrastructural visualization of the whole valves. We found multiple immune cells (Figure 3A) including canonical macrophages (Figure 3B), foam cells (Figure 3C), multinucleated giant cells (Figure 3D), and neutrophils (Figure 3E) within the BHVs, whereas calcified AVs were devoid of the 2 latter cell populations (Figure 3F).

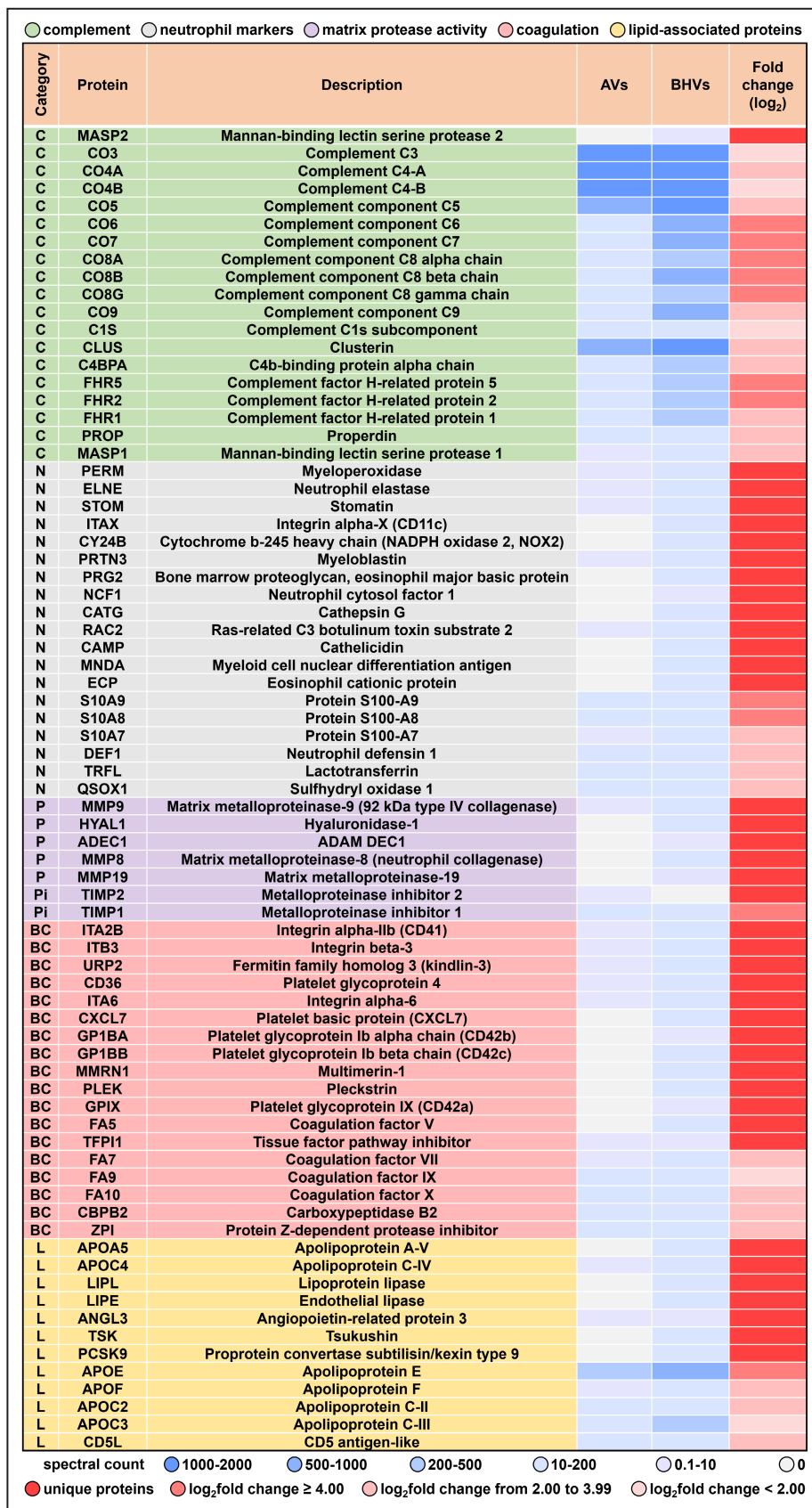
Indeed, most of the invading host cells in both XAP-BHVs and XPB-BHVs expressed pan-leukocyte marker

cluster of differentiation (CD) 45 as well as macrophage marker CD68 or neutrophil markers MPO and NE/ELA2, reflective of persistent inflammation (Figure 4). In addition, we detected T cells (CD3⁺), albeit in lower quantities and primarily in association with neutrophils, whereas CD19⁺ B cells were rarely observed. In contrast, calcified AVs were positively stained only for CD45, CD68, and CD3 (Figure 4). Semiquantitative image analysis indicated considerable differences in the neutrophil count between the BHVs and AVs, while respective counts of other immune cell populations did not differ significantly (Tables S4 and S5). These findings explained relative enrichment of the BHVs with neutrophil-related proteins and absence of such differences regarding macrophage markers, as macrophages invaded both BHVs and AVs. In addition, Western blotting for MPO and NE/ELA2 confirmed the abundant expression of these neutrophil markers in the BHVs (Figure S2A and S2B).

Enrichment of BHVs by complement components, in particular those of membrane attack complex, in combination with neutrophil invasion suggested an asymptomatic colonization with infectious agents; although none of the patients have shown any signs or symptoms of infective endocarditis, echocardiography did not reveal any vegetations, and blood inoculation was negative in all cases. We then carried out Gram and periodic acid-Schiff stainings of the excised BHVs and found small to moderate amounts of bacteria in 9

Figure 2. Annotation of unique or upregulated proteins in XAP-BHVs and XPB-BHVs.

The list of 75 selected proteins that have been unique or differentially expressed between the AVs and BHVs (XAP-BHVs and XPB-BHVs were pooled for this analysis as their proteomic profiles were similar on PLS-DA and volcano plot). AVs indicates aortic valves; PLS-DA, partial least squares discriminant analysis; XAP-BHVs, xenoaortic porcine bioprosthetic heart valves; and XPB-BHVs, xenopericardial bovine bioprosthetic heart valves.



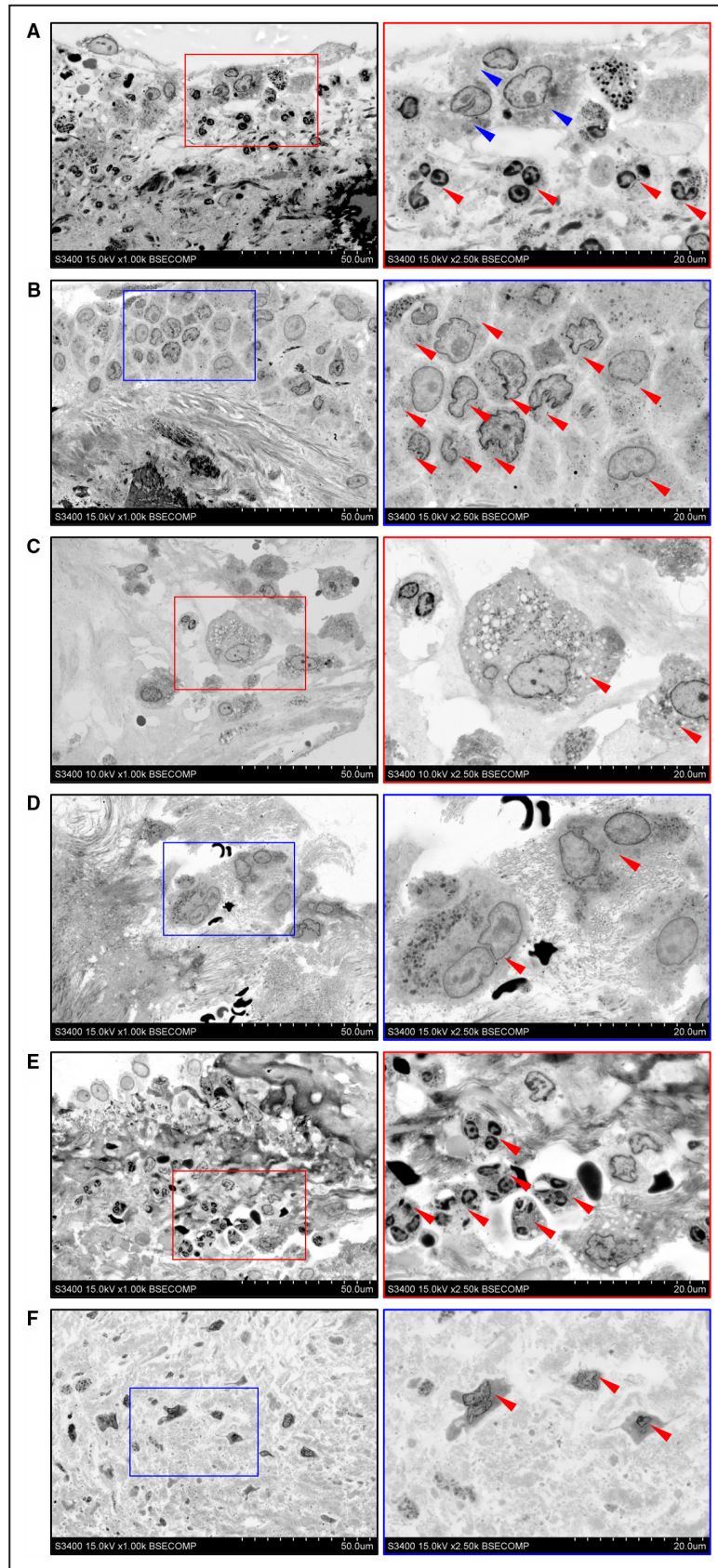


Figure 3. Immune cell populations inhabiting the BHVs and calcified AVs.

A, Both macrophages (indicated by blue arrows) and neutrophils (indicated by red arrows) were among the frequent findings in the BHVs, often being colocalized with each other. **B**, Canonical macrophages (indicated by red arrows) infiltrating the BHV. **C**, Foam cells (indicated by red arrows) formed because of excessive lipid load in the BHVs. **D**, Multinucleated giant cells (indicated by red arrows) reflecting the ECM degradation have been observed exclusively in the BHVs. **E**, Multiple neutrophils (indicated by red arrows) also were commonly found in the BHVs. **F**, Among all immune cells, calcified AVs contained only canonical macrophages (shown in the figure, indicated by red arrows) and foam cells, while multinucleated giant cells and neutrophils have not been detected. Images to the right are the close-ups of those to the left (demarcated by red or blue contour). EM-BSEM, representative images, magnification: $\times 1000$ (left) and $\times 2500$ (right), scale bars: $50\ \mu\text{m}$ (left) and $20\ \mu\text{m}$ (right). Accelerating voltage: 10 kV (**C**) or 15 kV (**A**, **B**, **D–F**). AVs indicates aortic valves; BHVs, bioprosthetic heart valves; ECM, extracellular matrix; and EM-BSEM, embedding and backscattered scanning electron microscopy.

of 10 samples (Figure 5A), albeit fungi have not been detected (Figure S3A through S3C). Bacteria were generally located below the surface, among the loosened and degraded collagen fibers (Figure 5A), but did not form any vegetations and were rarely colocalized with immune cells (Figure 5B and 5C). In contrast with the positive control (a valve suffering from prosthetic endocarditis, Figure 5D), BHV excised because of the rapid immunothrombosis (Figure 5E) or nonimplanted bovine pericardium (Figure 5F) did not contain signs of bacterial contamination. Following the isolation of DNA from the BHV or AV fragments, polymerase chain reaction tests verified *Streptococcus* spp. infection in half of the BHVs but not the AVs (Table S4 and S5). Hence, we concluded that asymptomatic bacterial inroad, presumably attributable to the transient bacteremia, was the cause behind the neutrophil and complement attacks observed in both XAP-BHVs and XPB-BHVs.

Bioprosthetic Heart Valves Deteriorate Because of Uncurbed Proteolysis

Disintegration of the ECM, an essential cause of SVD, is often associated with the disrupted balance between matrix-degrading enzymes (eg, MMPs) and their tissue inhibitors (eg, TIMPs). As soon as we detected numerous proteases (NE/ELA2, PRTN3, cathepsin G, MMP-8/9) overrepresented in the BHVs concurrently with downregulated metalloproteinase inhibitors (TIMP-1/2) in comparison with calcified AVs, we then profiled the BHV and AV lysate for 35 proteases and 32 protease inhibitors. Densitometry analysis showed the increased levels of PRTN3, MMP-8/9, and urokinase (Figure 6 and Figure S4) and reduced levels of TIMP-1/2 (Figure 7 and Figure S4) in the BHVs as compared with the AVs. Further, membrane-anchored glycoprotein reversion-inducing-cysteine-rich protein with Kazal motifs, a negative regulator of MMP-9, was upregulated in the AVs in contrast with the BHVs (Figure 7 and Figure S4). No statistically significant differences have been identified between XAP-BHVs and XPB-BHVs (Figures 6 and Figure 7, and Figure S4). Dot blotting of the nonimplanted bovine pericardium demonstrated a minor nonspecific binding, attesting to the reliability

of the results (Figure S4). Collectively, these findings confirmed the data obtained from the proteomic profiling and provided evidence toward the uncontrolled proteolysis in XAP-BHVs and XPB-BHVs, potentially underlying SVD.

Both Immune Cells and Plasma Are Stakeholders in Proteolysis Within the BHVs

We then focused on identifying the sources of proteases emerging in BHVs and contributing to SVD. Elevated levels of neutrophil-related and plasma-associated proteases suggested that different proteases enriched in the BHVs may be of distinct origin. To challenge this hypothesis, we performed a series of immunohistochemical stainings for the number of matrix metalloproteinases (MMP-1/2/8/9/12) and their tissue inhibitors (TIMP-1/2). Most of the indicated proteases were detected in all BHVs and AVs (Figure 8). Intriguingly, the XPB-BHV that failed because of immunothrombosis 2 days after implantation contained high amounts of cell-associated MMP-8 and showed diffuse MMP-9 expression within the clot, testifying to the neutrophil origin of MMP-8 and plasma origin of MMP-9 (Figure 8). In concert with the ultra-high-performance liquid chromatography–tandem mass spectrometry and western or dot blotting data, MMP-8 was better expressed in the BHVs, as it is largely produced by neutrophils (Figure 8). All MMPs and TIMPs including MMP-9 were colocalized with the cells in the AVs (Figure 8). In the BHVs, positive staining for MMP-1/2/8/12 and TIMP-1/2 was colocalized with the immune cells (Figure 8), whereas MMP-9 exhibited the sharpest staining within the spongiosa (in XAP-BHVs, Figure 9A) and was associated with the degraded ECM beneath the surface (in XPB-BHVs, Figure 9B). Combined staining for NE/ELA2 and MMP-8 confirmed the localization of MMP-8 near the neutrophils inhabiting XAP-BHVs and XPB-BHVs (thresholded Mander's split colocalization coefficient=0.6) along with the absence of its expression in the distant ECM as well as in the AVs (Figure 10A). In contrast, MMP-9 was ubiquitously expressed in the BHVs and was abundantly represented in the degraded

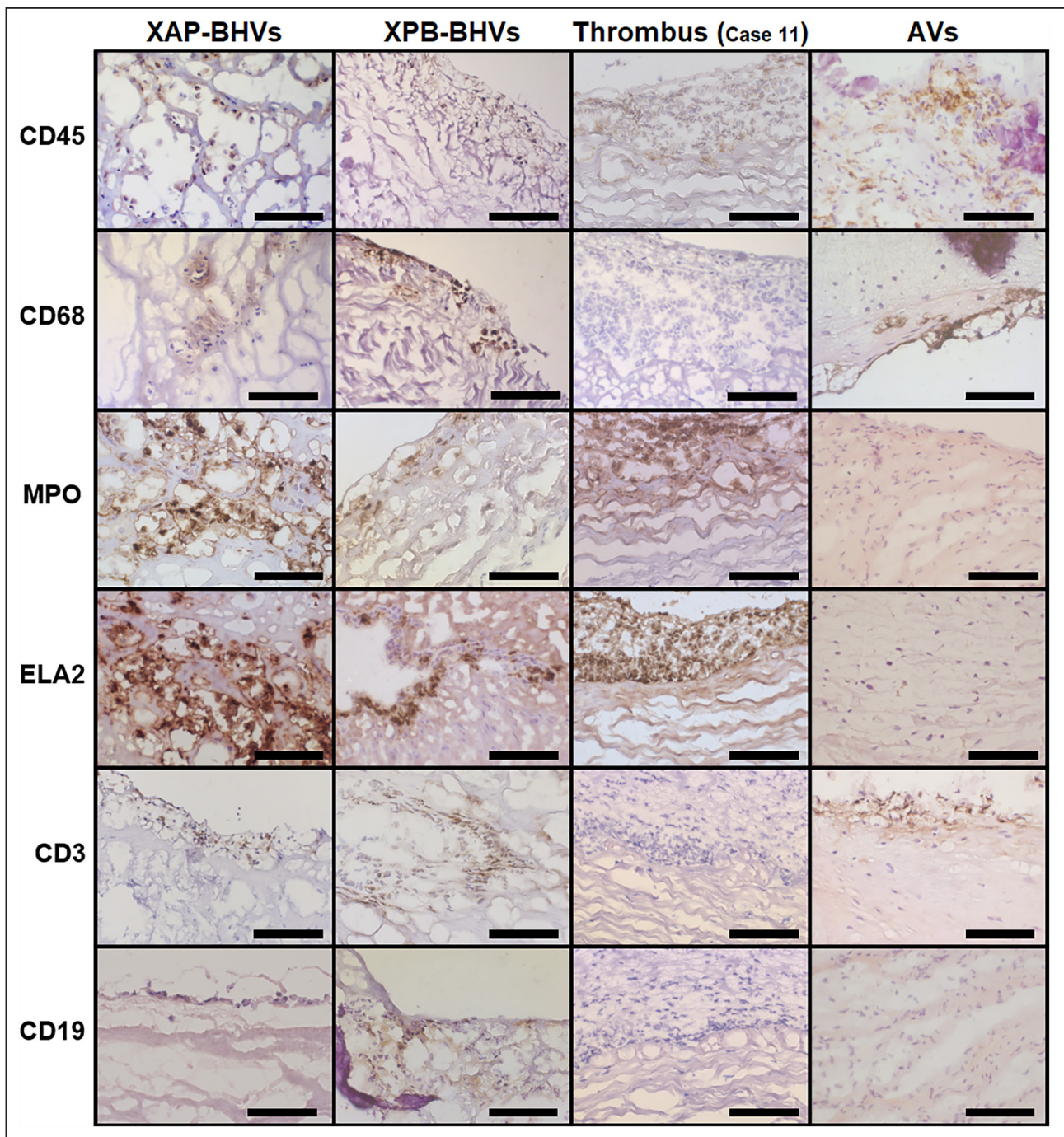


Figure 4. Macrophages and neutrophils are prevailing cell populations in BHVs while calcified AVs are devoid of neutrophils. Cells infiltrating XAP-BHVs and XPB-BHVs were positively stained (brown color) for pan-leukocyte marker CD45, macrophage marker CD68 and neutrophil markers MPO and NE/ELA2, with rare T (CD3⁺) and no B (CD19⁺) cells. Prosthetic thrombus served as a positive control for CD45, MPO, and NE/ELA2 stainings. AVs contained only CD45⁺, CD68⁺, and CD3⁺-positive cells. Immunohistochemical staining, representative images, magnification: $\times 400$, scale bar: 100 μm . AVs indicates aortic valves; BHVs, bioprosthetic heart valves; CD, cluster of differentiation; MPO, myeloperoxidase; NE/ELA2, neutrophil elastase; XAP-BHVs, xenoaortic porcine bioprosthetic heart valves; XPB-BHVs, xenopericardial bovine bioprosthetic heart valves.

ECM regions (Figure 10A). Semiquantitative image analysis confirmed an increased MMP-9 expression in both XAP-BHVs and XPB-BHVs in comparison with the calcified AVs (Figure 10B).

Hence, the expression pattern of MMP-9 in the BHVs was strikingly different from those of other measured MMPs and TIMPs, as MMP-9 positive staining was mostly restricted to the loosened or disorganized ECM

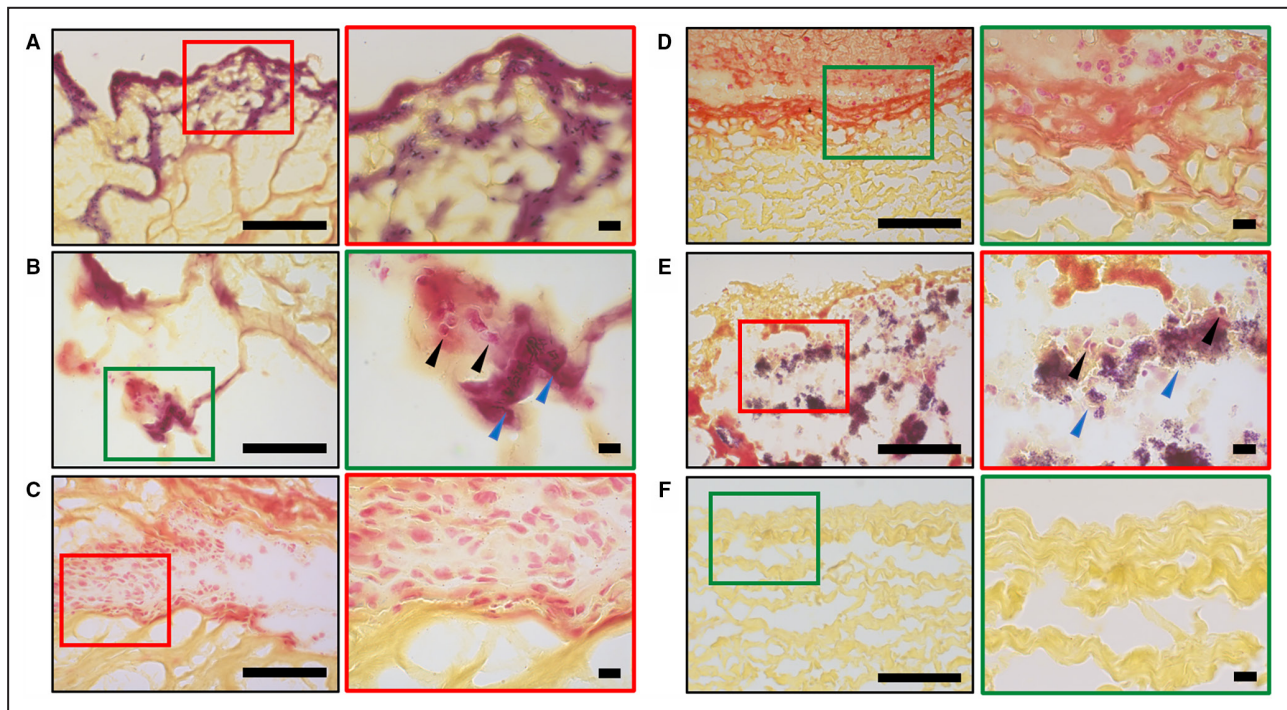


Figure 5. Bacterial colonization of XAP-BHVs and XPB-BHVs.

A, Moderate amounts of spherical and rodlike bacteria beneath the BHV surface. **B**, Colocalization of immune cells (indicated by black arrows) and bacteria (indicated by blue arrows) has been rarely observed. **C**, Immune cells were mostly located in bacteria-free areas. **D**, BHV-associated thrombotic masses have been heavily infiltrated with neutrophils but were devoid of bacteria. **E**, Vegetations in the BHV suffering from the prosthetic endocarditis caused by *Staphylococcus aureus* (positive control). **F**, Nonimplanted bovine pericardium used as a negative control to exclude an accidental contamination. Note the large bacterial colonies (indicated by blue arrows) and aggressive infiltration by immune cells (indicated by black arrows). Images to the left (demarcated by red or green contour). Gram staining, magnification: $\times 400$ (left) and $\times 1000$ (right), scale bars: $100\mu\text{m}$ (left) and $10\mu\text{m}$ (right). XAP-BHVs indicates xenoaortic porcine bioprosthetic heart valves; and XPB-BHVs, xenopericardial bovine bioprosthetic heart valves.

of the dysfunctional BHVs and to the associated thrombi, pointing at the blood as the main source of MMP-9 in the degraded prosthetic tissue. Conversely, TIMP-1/2 was notable neither in the ECM of failing BHVs nor in BHV-associated thrombotic masses. Given the abundance of TIMP-1/2 in the AVs and their cellular localization, this infers that TIMPs in the BHVs are produced by invading host cells, which are relatively scarce and unable to produce sufficient quantities of TIMPs to properly counteract the high amount of cell- and blood-derived proteases. Therefore, we proposed that both plasma- and neutrophil-derived proteases, enhanced by an inherent deficiency of their respective inhibitors, are the culprits of uncurbed proteolysis within the BHVs and therefore have the causative role in the development of SVD.

XAP-BHVs and XPB-BHVs Fail Regardless of Cellular Infiltration and Lipid Deposition, Indicating the Main Role of Plasma-Derived Proteases in SVD

Having elucidated the reasons behind the SVD, we then investigated the relative impact of plasma- and

neutrophil-derived proteases. Almost all excised BHVs were invaded by host cells and suffered from loosening, degradation, and fragmentation of the ECM (Table S2). While XAP-BHVs displayed moderate (Figure S5A) to severe (Figure S5B) cellular infiltration that frequently involved the whole valve and was associated with calcium deposits or perforations, XPB-BHVs contained minor amounts of cells located at or underneath the surface (Figure S6A), and XPB-BHV that failed because of rapid thrombosis was devoid of any cells, although the clot included multiple neutrophils (Figure S6B, previously described in detail²³).

Russell-Movat's pentachrome staining of XAP-BHVs and XPB-BHVs showed that the ECM fibers were composed of collagen but not glycosaminoglycans, although they were detected around invading host cells (Figure S7A) and in the pathological connective tissue grown on the BHV (pannus; Figure S7B). Intriguingly, fibrin clots were frequently detected at the BHV surface (Figure S7C and S7D) that was in line with the high abundance of coagulation- and platelet-associated proteins in the BHVs. Concurring with these findings, nonimplanted XAP-BHVs and XPB-BHVs consisted

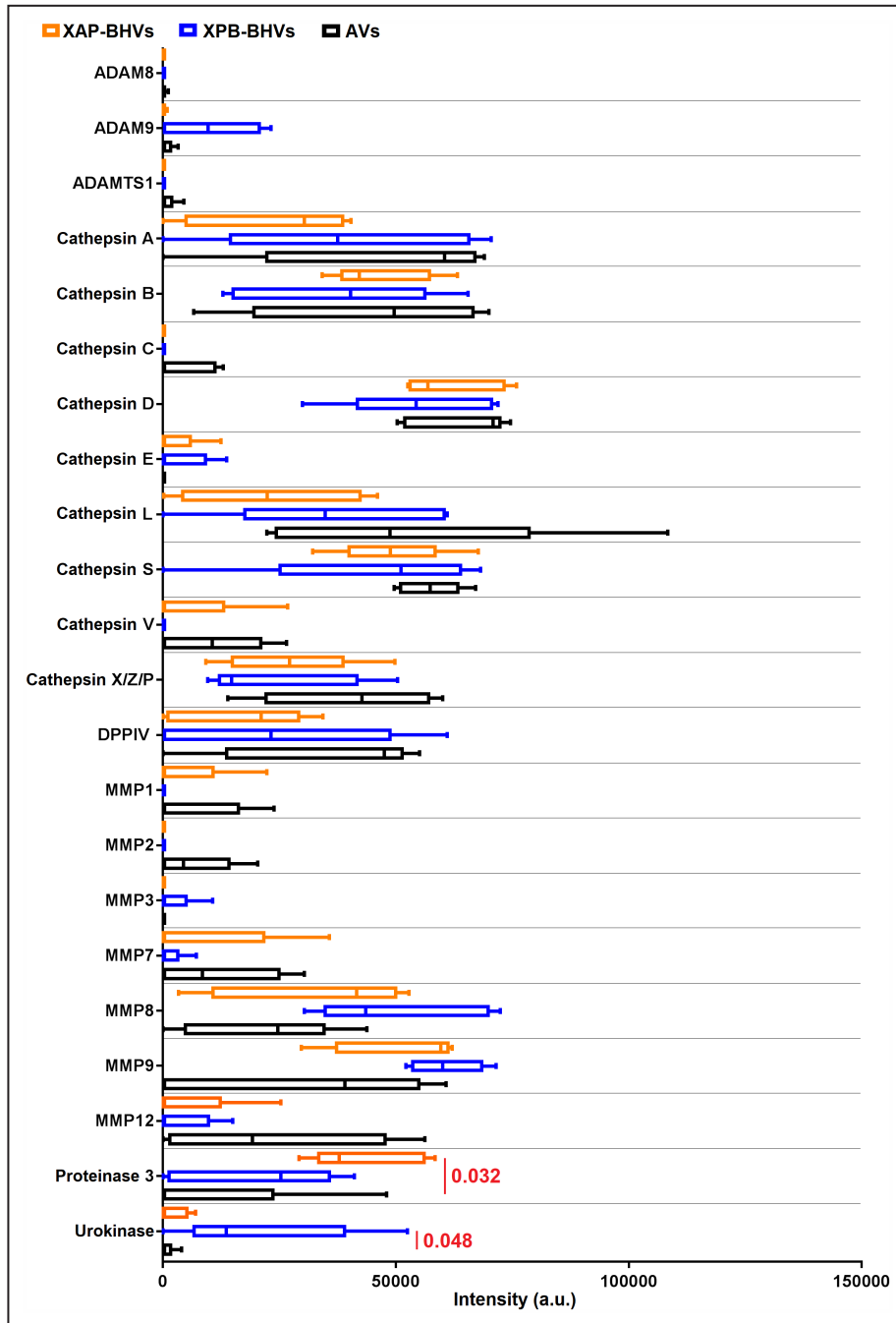


Figure 6. Densitometry analysis (ImageJ) of protease levels in XAP-BHVs, XPB-BHVs, and calcified AVs.

Box-and-whisker plot, center lines indicate median, boxes bounds indicate 25th–75th percentiles, whiskers indicate range. Kruskal–Wallis test with post hoc FDR adjustment for multiple comparisons by 2-stage linear step-up procedure of Benjamini, Krieger, and Yekutieli. Statistically significant, FDR-corrected q values are provided above boxes. AVs indicates aortic valves; FDR, false discovery rate; XAP-BHVs, xenoaortic porcine bioprosthetic heart valves; and XPB-BHVs, xenopericardial bovine bioprosthetic heart valves.

exclusively of collagen (Figure S7E and S7F), and positive platelet and fibrin immunostaining confirmed successful clot identification by means of Russell-Movat’s pentachrome staining (Figure S7G and S7H).

Lipid retention was documented in all XAP-BHVs, most of which were notable for the fatty streaks/spots or massive lipid deposition (Figure S8A) as well as foam cells (Figure S8B). On the contrary, the vast

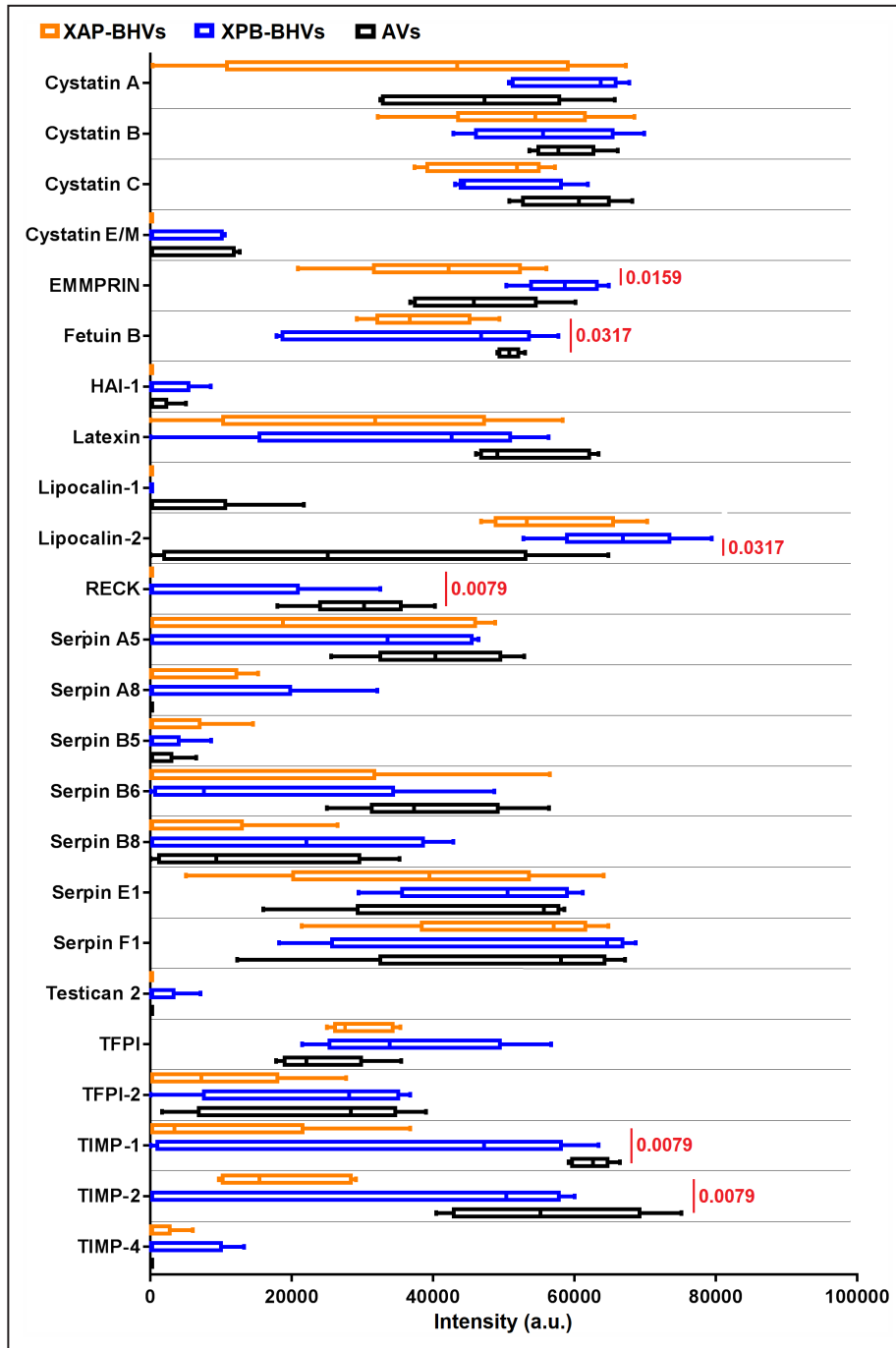


Figure 7. Densitometry analysis (ImageJ) of protease inhibitor levels in XAP-BHVs, XPB-BHVs, and calcified AVs.

Box-and-whisker plot, center lines indicate median, boxes bounds indicate 25th to 75th percentiles, whiskers indicate range. Kruskal–Wallis test with post hoc FDR adjustment for multiple comparisons by 2-stage linear step-up procedure of Benjamini, Krieger, and Yekutieli. Statistically significant, FDR-corrected *q* values are provided above boxes. ADAM indicates a disintegrin and metalloproteinase; ADAMTS, a disintegrin and metalloproteinase with thrombospondin motifs; AVs, aortic valves; DPPIV, dipeptidyl peptidase 4; EMMPRIN, extracellular matrix metalloproteinase inducer; FDR, false discovery rate; HAI-1, hepatocyte growth factor activator inhibitor 1; MMP, matrix metalloproteinase; RECK, reversion-inducing-cysteine-rich protein with Kazal motifs; TFPI, tissue factor pathway inhibitor; TIMP, tissue inhibitor of metalloproteinases; XAP-BHVs, xenoaortic porcine bioprosthetic heart valves; and XPB-BHVs, xenopericardial bovine bioprosthetic heart valves.

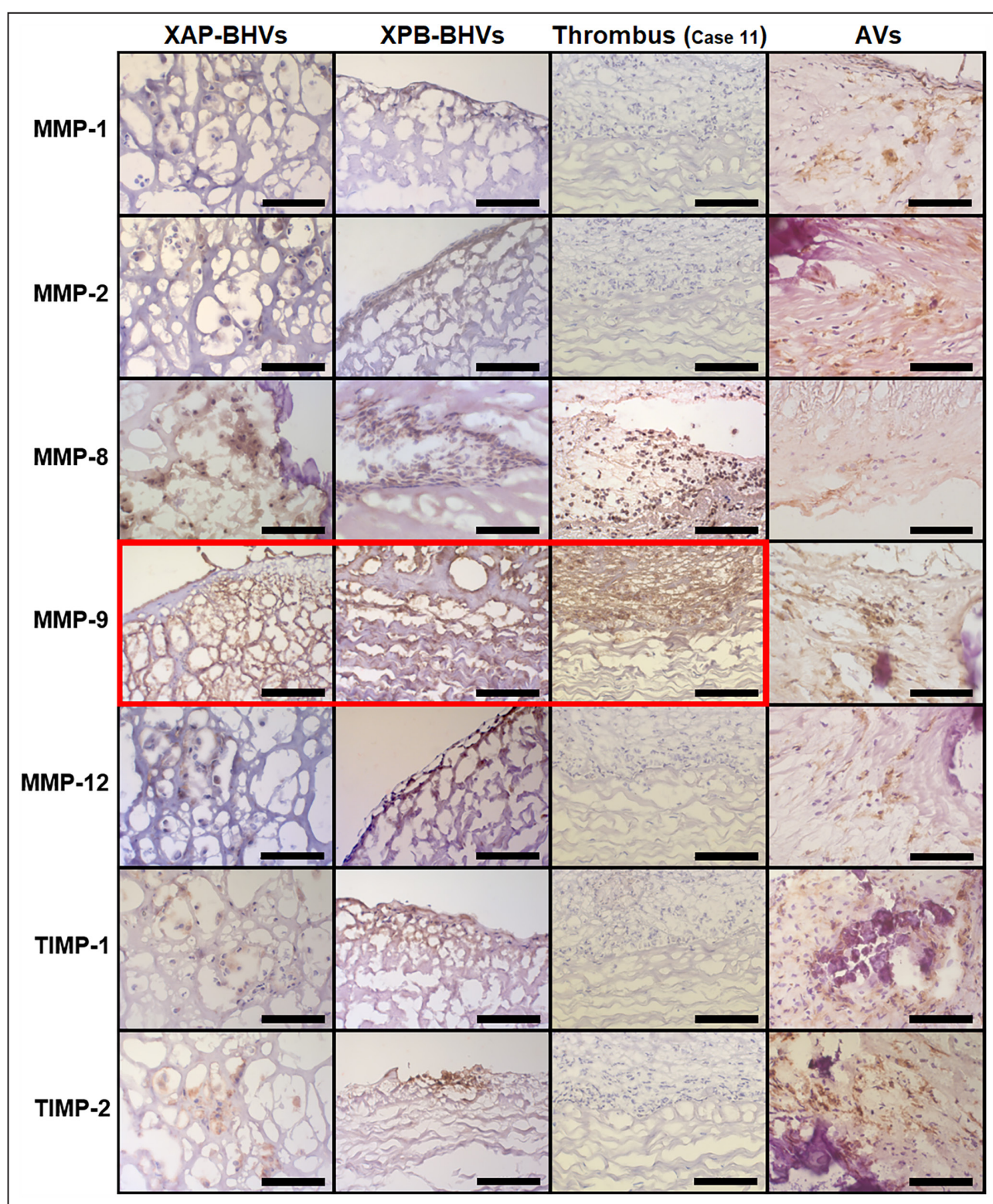


Figure 8. Expression patterns of MMPs/TIMPs within failing BHVs and calcified AVs.

All proteases and protease inhibitors (brown color) were colocalized with cells except for the MMP-9 within the BHVs, which has been colocalized with the degraded extracellular matrix. Note that MMP-8 and MMP-9 are abundant within the clot in the BHV diagnosed with immunothrombosis and excised as early as 2 days postimplantation, indicating neutrophils as the principal source of MMP-8 (colocalized with the cells) and plasma as the primary source of MMP-9 (diffuse staining pattern). Immunohistochemical staining, magnification: $\times 400$, scale bar: $100\ \mu\text{m}$. AVs indicates aortic valves; BHVs, bioprosthetic heart valves; MMP, matrix metalloproteinase; and TIMPs, tissue inhibitors of metalloproteinases.

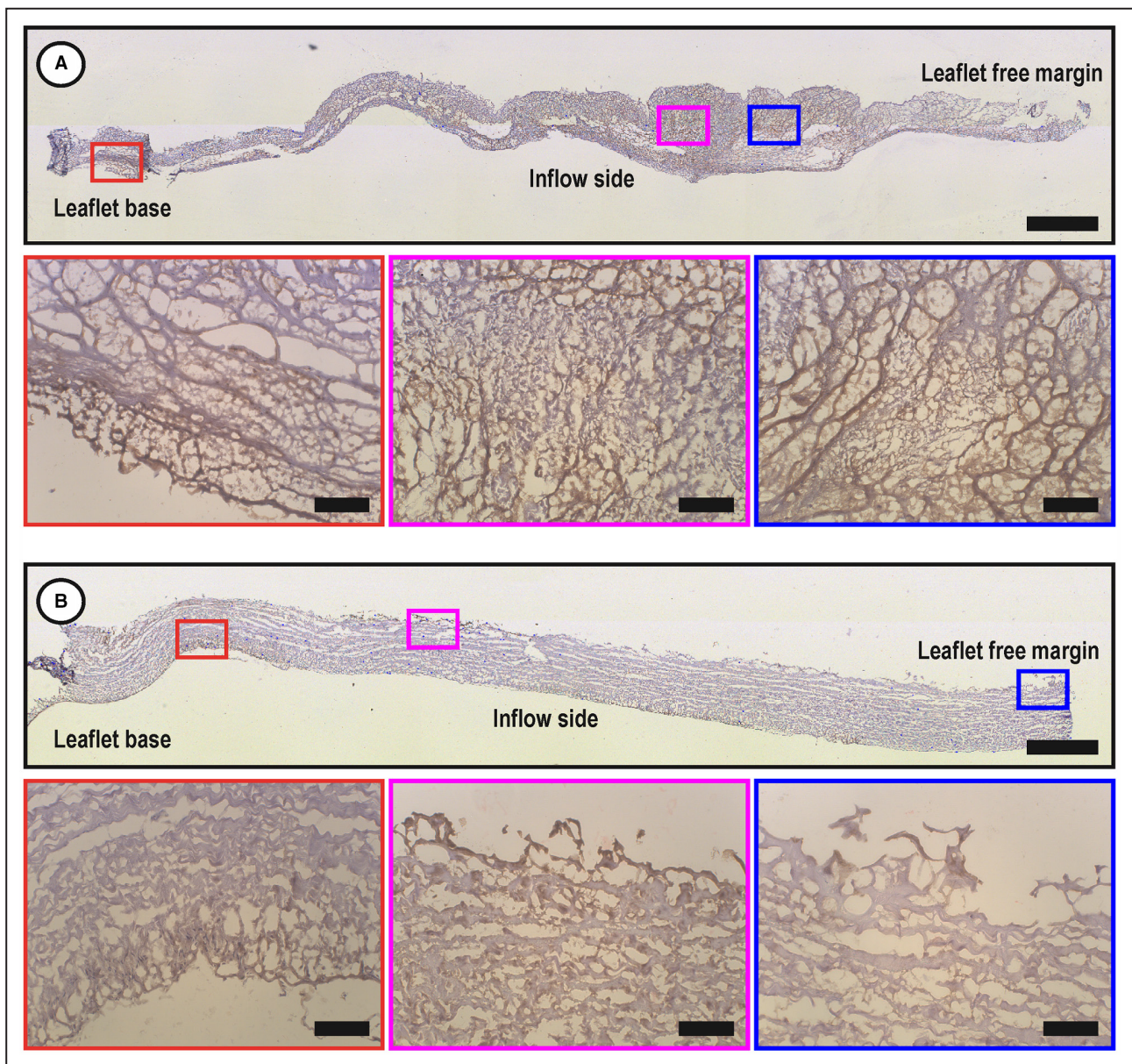


Figure 9. MMP-9 is colocalized with the spongiosa and degraded extracellular matrix of failing BHVs.

A, XAP-BHVs, note the highest MMP-9 expression (brown color) in the spongiosa. **B**, XPB-BHVs, note the highest MMP-9 expression in the degraded extracellular matrix beneath the surface. For **A** and **B**: images below are the close-ups of the image above (demarcated by red, purple, or blue contour). Immunohistochemical staining, magnification: $\times 50$ (overview, merged image), scale bar: $1000\mu\text{m}$ (overview) and magnification: $\times 200$, scale bar: $100\mu\text{m}$ (close-ups). MMP-9 indicates matrix metalloproteinase 9; XAP-BHVs, xenoaortic porcine bioprosthetic heart valves; and XPB-BHVs, xenopericardial bovine bioprosthetic heart valves.

majority (4/5) of XPB-BHVs did not demonstrate any signs of lipid retention, and the remaining one showed small lipid spots below the surface (Figure S8C). Nonimplanted XAP-BHVs and XPB-BHVs were also negatively stained (Figure S8D). Therefore, patterns of lipid and cellular infiltrations intercorrelated, indicating a pathogenetic link between these lesions, as XAP-BHVs displayed high amounts of cellular invasion and lipid deposition in contrast to XPB-BHVs. Microcalcifications were colocalized with the invading

host cells (Figure S9A) or located separately in the ECM (Figure S9B), suggesting involvement of dystrophic calcification in the mineralization of XAP-BHVs and XPB-BHVs through the passive deposition of Ca^{2+} ions on both cell debris and degraded ECM components.

Although XAP-BHVs showed moderate to severe infiltration by immune cells and pronounced lipid deposition, as opposed to XPB-BHVs, which exhibited significantly lesser cellular inroad and lipid load, all these prostheses eventually suffered from SVD with

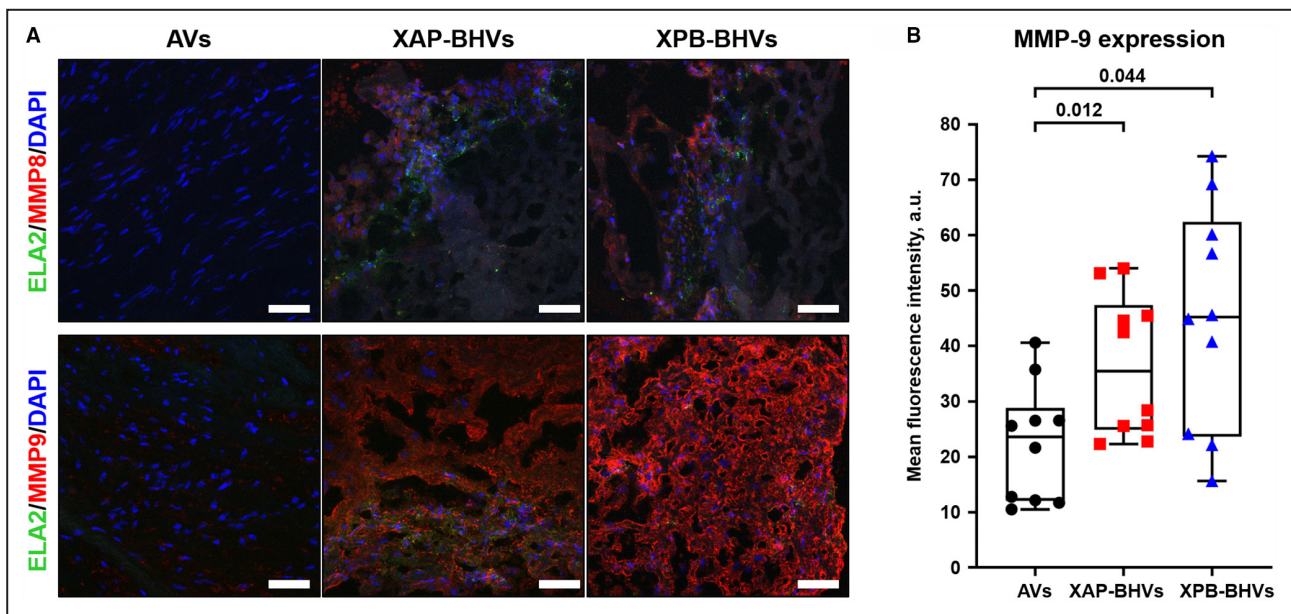


Figure 10. Immunofluorescence analysis of MMP-8 and MMP-9 expression in calcified AVs, XAP-BHVs, and XPB-BHVs.

A, Combined immunofluorescence staining for the neutrophil marker NE/ELA2 (green color) either with neutrophil-secreted MMP-8 or with plasma-derived MMP-9 (red color). Nuclei are counterstained with DAPI (blue color). Representative images. Note the colocalization of MMP-8 with NE/ELA2 and ubiquitous staining pattern of MMP-9. Magnification: $\times 200$, scale bar: $50\mu\text{m}$. **B**, Semiquantitative analysis of mean fluorescence intensity (MMP-9, red channel) in confocal images ($n=10$ per group). Box-and-whisker plot combined with univariate scatterplot, center lines indicate median, boxes bounds indicate 25th–75th percentiles, whiskers indicate range. Each dot reflects a measurement from 1 image of a prosthetic or native valve. Kruskal–Wallis test with post hoc false discovery rate (FDR) adjustment for multiple comparisons by 2-stage linear step-up procedure of Benjamini, Krieger, and Yekutieli. Statistically significant, FDR-corrected q values are provided above boxes. AVs indicates aortic valves; DAPI, 4',6-diamidino-2-phenylindole; FDR, false discovery rate; MMP, matrix metalloproteinase; NE/ELA2, neutrophil elastase; XAP-BHVs, xenoaortic porcine bioprosthetic heart valves; and XPB-BHVs, xenopericardial bovine bioprosthetic heart valves.

similar proteomic signatures. This highlights a key role of plasma-derived proteases such as MMP-9 in BHV failure, though cell- (eg, neutrophil-) secreted proteases also seem to contribute significantly to this pathology.

DISCUSSION

Here, we performed a comprehensive analysis of SVD causes in the EGDE-treated BHVs, which represent the next step toward better safeguarding from mineralization in comparison with glutaraldehyde-treated BHVs but still suffering from SVD.^{12–15,24} To better investigate the pathophysiological scenario in this SVD setting, we interrogated 2 types of failed EGDE-treated BHVs: XAP-BHVs prepared from the entire porcine leaflets and XPB-BHVs fabricated from the bovine pericardium, both withdrawn at the repeated heart valve replacement surgery. With the aim to differentiate CAVD and SVD causes, we compared XAP-BHVs and XPB-BHVs with the calcified AVs excised from the patients with CAVD during the primary heart valve replacement.

Unbiased proteomic profiling of XAP-BHVs, XPB-BHVs and calcified AVs revealed 5 major protein categories overrepresented in XAP-BHVs and XPB-BHVs,

without any significant differences between these 2 BHV types: complement components, neutrophil markers, matrix proteases, platelet markers and coagulation factors, and proteins involved in the lipid metabolism. Different immunostaining and Western blotting varieties confirmed overexpression of several neutrophil markers (MPO, NE/ELA2, PRTN3, MMP-8) and plasma-derived proteases (MMP-9) in the BHVs and downregulation of specific tissue protease inhibitors (TIMP-1/2) in the BHVs as compared with the AVs. Electron microscopy examination found moderate to severe neutrophil invasion in the BHVs, which, in combination with upregulated complement response, suggested occult bacterial colonization of the prosthetic tissue (as all patients were free of clinical and echocardiographic signs and symptoms of infective endocarditis). Gram staining of the BHV sections and polymerase chain reaction analysis of homogenized BHV segments confirmed streptococcal contamination of prosthetic tissues, which ostensibly provoked neutrophil attack and subsequent release of the respective proteases.

Despite neutrophil invasion and complement activation culminated by the membrane attack complex formation developed in response to the bacterial colonization, neutrophils and macrophages were frequently

located aside from bacterial colonies, suggesting additional causes of immune cell recruitment. The indicated triggers might include native xenogeneic epitopes such as galactose- α -1,3-galactose and N-glycolylneuraminic acid as well as neoepitopes formed by citrullination. Previously, it has been shown that galactose- α -1,3-galactose and N-glycolylneuraminic acid cause immune rejection of xenogeneic transplants,^{25,26} including glutaraldehyde-treated BHVs.^{27,28} However, Russell-Movat's pentachrome staining did not detect any glycosaminoglycans in the control leaflets of XPB-BHVs that have not been implanted. In addition, we investigated ultra-high-performance liquid chromatography–tandem mass spectrometry data for the presence of citrullinated peptides and identified 122 citrullinated proteins, yet only 2 citrullinated peptides among them were exclusively presented in the BHVs. Collectively, these observations do not support autoimmune response as a major factor impacting the development of SVD in the EGDE-treated BHVs, indirectly pointing to the bacteria as the primary cause of neutrophil infiltration.

Importantly, cell-secreted and plasma-derived proteases had a distinct distribution pattern across the prosthetic tissue. Although MMP-9 was expressed ubiquitously in the BHVs, it was particularly abundant in the degraded prosthetic ECM, while other proteases, as well as TIMP-1/2, were colocalized with the immune cells. Notably, MMP-9 was also prominent in the prosthetic clot, forming as soon as 2 days after implantation and leading to the repeated valve replacement.²³ These findings indicated plasma as an essential source of MMP-9 and pinpointed MMP-9 (and probably other plasma-derived proteases such as urokinase) as a principal culprit of SVD along with the significant role of numerous neutrophil-derived proteases (NE/ELA2, PRTN3, MMP-8, cathepsin G), which were upregulated in the BHVs because of persistent bacterial contamination. Given that plasma- and neutrophil-derived proteases were ample in the BHVs (in contrast with the AVs) and TIMP-1/2 was not notable in the degraded ECM and prosthetic clots although being highly presented in the AVs, this suggested an inability of tissue inhibitors to halt the proteolytic activity in the BHVs. Damaged by blood proteases, ECM niches become a convenient site for bacterial invasion, which triggers an immune cell attack. Having considered the data from the Russell-Movat's pentachrome staining of the sections from snap-frozen BHVs, immunohistochemical staining from the corresponding serial sections, and proteomic profiling, we suggested that the fibrin clots on the BHV surface represent a portal of entry for the asymptomatic bacterial colonization. An overrepresentation of coagulation-specific proteins (ie, platelet markers and coagulation factors) in the BHVs supports this hypothesis. As soon as bacteria successfully

adhere to the clots formed on the BHV surface and a few layers beneath, they are able to invade further, being protected from shedding. Proliferation of bacteria is then supplied by the circulating blood leaking through the degraded ECM within the BHVs.

Uncontrolled proteolysis leads to the irreversible damage, degradation, and disintegration of the prosthetic ECM, ultimately resulting in SVD, calcification, and BHV failure. Notably, proteolytic degradation is significantly enhanced by the cyclic hemodynamic load exerted on the BHVs during the cardiac cycle. Accelerated cyclic fatigue promotes the unwinding and degradation of type I collagen within the BHVs, in particular upon treatment with bacterial collagenase or trypsin, and results in loss of glycosaminoglycans from the ECM.^{29,30} Such collagen degradation significantly affects the mechanical properties of BHVs.³¹ While the deterioration of collagen fibers during the enzymatic stress begins rapidly, cyclic tensile loading provokes their reorientation, which further leads to the uneven distribution of hemodynamic stress, thereby promoting ECM disintegration.³² This issue is crucially important as the improper fiber architecture within the bioprosthetic ECM considerably impacts their life span, and fibers oriented perpendicular to the loading direction generally fail faster than those aligned along the loading direction.³³ This issue was extensively discussed in the review by Sacks,³⁴ where he stated the need in the next-generation chemical fixation approaches to retain the integrity of the bioprosthetic ECM, extend BHV durability, and prolong their functioning. Earlier, neomycin-treated glutaraldehyde-fixed BHVs showed increased resistance to proteolytic degradation and preserved glycosaminoglycans after both enzymatic stress, that is, treatment with type VII collagenase, elastase, hyaluronidase, and chondroitinase, and mechanical load during *in vitro* accelerated cyclic fatigue testing.^{35,36} The interactions between the MMPs and the cross-linked ECM have been vaguely examined to date, though it was noted that fixation of the prosthetic tissue using glutaraldehyde or EGDE does not furnish its complete protection from enzymatic degradation.^{37,38} Recent papers revealed the deleterious effects of oxidative degradation, mediated by macrophage- and neutrophil-derived reactive oxygen species and MPO, for the prosthetic ECM.^{39,40} Emergence of plasma-derived proteases in glutaraldehyde-fixed BHVs has not been scrutinized hitherto.

Unexpectedly, XAP-BHVs, which have been implanted in younger patients and are more permeable because of the degrading glycosaminoglycans of the spongiosa,^{41,42} had longer life span as compared with XPB-BHVs in spite of the remarkable immune cell infiltration and lipid deposition, suggesting these processes are important but not pivotal for the development of SVD in EGDE-treated BHVs, in contrast with

the precipitation of plasma-derived proteases such as MMP-9. Moreover, microcalcifications frequently were not colocalized with invading host cells, underscoring the role of dystrophic calcification in the SVD pathogenesis in EGDE-treated BHVs.⁴³ Together, this highlights the key role of the plasma-derived proteases that shape the prosthetic ECM toward a procalcific micro-environment and hence enhance the mineralization of the BHVs.

Among the limitations of our study was the inability to obtain normally functioning EGDE-treated BHVs (eg, from patients who died from causes not related to cardiovascular disease), which could be used as negative controls to compare with failed BHVs. Unfortunately, such patients are not admitted to our clinic, and therefore obtaining such BHVs has been barely possible. Further, we did not compare the proteomic profiles of AV regurgitation and BHV failure, 2 pathologies caused by a critical decrease in the ECM stiffness, to differentiate their pathophysiological mechanisms.

To conclude, emergence of multiple neutrophil-secreted proteases, colocalization of abundant plasma-derived MMP-9 with the degraded ECM, microthrombosis, and microcalcifications in the disintegrated ECM aside the host cells indicate proteolytic degradation and dystrophic calcification as the main culprits of failure of EGDE-treated BHVs. Future investigations may extend the set of plasma-derived proteases responsible for the development of SVD and focus on the development of the protective envelope shielding the BHVs from the bacterial and immune cell invasion as well as precipitation of the proteases. The rationale behind this approach is that such sheath would protect the BHV from the enzyme precipitation (regardless of whether the enzymes are produced by bacteria or host cells or emerge from the blood), bacterial invasion (as the polymer sheath repels fibrin as soon as it is hydrophilic and has zero thrombogenicity), cellular infiltration (as polymer physically blocks the pores within the ECM where cells can attach, migrate, and reside), and calcium deposition (as blood, which is the primary source of Ca²⁺ ions mediating the calcification, does not leak into the BHV because it cannot permeate the polymer occluding the hollows and pores in the bioprosthetic ECM). Regarding the chemical composition, we suggest that the polymer must be hydrophilic (to prevent clotting and thrombosis), bio-stable (to withstand the enzymatic stress), and strongly attached to the BHV to preclude the possible shedding at the cyclic pressure conditions. Wrapping of the BHV into such protective sheath can be placed immediately after the chemical fixation and must be performed under sterile conditions, as the existing fixatives such as glutaraldehyde or ethylene glycol diglycidyl ether also sterilize BHV. In a recent paper by Ding et al,⁴⁴ 2-amino-4-pentenoic acid was used to introduce

carbon-carbon double bonds into the glutaraldehyde-crosslinked porcine pericardium (ie, a co-crosslinking approach was applied), and then poly(ethylene glycol) diacrylate was immobilized on the pericardium by radical polymerization. In vitro studies showed 4-fold lower adhesion of platelets at the surface of modified BHVs and demonstrated their increased resistance to the collagenase-induced ECM degradation and calcification, although in vivo implantation has not been performed.⁴⁴ Further studies by this and other groups, employing both in vitro tests and in vivo studies (eg, an implantation of the enveloped BHVs into sheep), will provide an answer whether such an approach is able to protect BHVs from SVD.

ARTICLE INFORMATION

Received September 19, 2022; accepted November 28, 2022.

Affiliations

Department of Experimental Medicine, Research Institute for Complex Issues of Cardiovascular Diseases, Kemerovo, Russian Federation (A.E.K., T.V.G., E.A.O., L.A.B., D.K.S., V.E.M., M.A.A., R.A.M., E.A.V., T.N.A., M.A.R., A.N.S., A.V.E., L.S.B., A.G.K.); Department of Regenerative Biomedicine, Research Institute of Cytology, St. Petersburg, Russian Federation (A.A.L.); and Centre for Molecular and Cell Technologies, St. Petersburg State University Research Park, St. Petersburg State University, Universitetskaya Embankment, St. Petersburg, Russian Federation (B.R.Z.).

Sources of Funding

The clinical and experimental parts of this study were supported by the Russian Science Foundation grant 21-75-10107 (A. Kostyunin), <https://rscf.ru/en/project/21-75-10107/>. Ultra-high-performance liquid chromatography-tandem mass spectrometry with ion mobility and bioinformatic analysis were supported by the Russian Science Foundation grant 18-14-00152 (A. Lobov) (<https://rscf.ru/project/18-14-00152/>). Proteomics analyses were conducted in the Centre for Molecular and Cell Technologies, St. Petersburg State University Research Park. The study sponsors had no role in study design; in the collection, analysis, and interpretation of data; in the writing of the report; and in the decision to submit the paper for publication.

Disclosures

None.

Supplemental Material

Data S1
Tables S1–S5
Figures S1–S9

REFERENCES

- Otto CM, Nishimura RA, Bonow RO, Carabello BA, Erwin JP III, Gentile F, Jneid H, Krieger EV, Mack M, McLeod C, et al. 2020 ACC/AHA guideline for the management of patients with valvular heart disease: a report of the American College of Cardiology/American Heart Association joint committee on clinical practice guidelines. *Circulation*. 2021;143:e72–e227. doi: [10.1161/CIR.0000000000000923](https://doi.org/10.1161/CIR.0000000000000923)
- Lindman BR, Clavel MA, Mathieu P, Jung B, Lancellotti P, Otto CM, Pibarot P. Calcific aortic stenosis. *Nat Rev Dis Primers*. 2016;2:16006. doi: [10.1038/nrdp.2016.6](https://doi.org/10.1038/nrdp.2016.6)
- Bax JJ, Delgado V. Bioprosthetic heart valves, thrombosis, anticoagulation, and imaging surveillance. *JACC Cardiovasc Interv*. 2017;10:388–390. doi: [10.1016/j.jcin.2017.01.017](https://doi.org/10.1016/j.jcin.2017.01.017)
- Kostyunin AE, Yuzhalin AE, Ovcharenko EA, Kutikhin AG. Development of calcific aortic valve disease: do we know enough for new clinical trials? *J Mol Cell Cardiol*. 2019;132:189–209. doi: [10.1016/j.jmcc.2019.05.016](https://doi.org/10.1016/j.jmcc.2019.05.016)

5. Head SJ, Çelik M, Kappetein AP. Mechanical versus bioprosthetic aortic valve replacement. *Eur Heart J*. 2017;38:2183–2191. doi: [10.1093/eurheartj/ehx141](https://doi.org/10.1093/eurheartj/ehx141)
6. Capodanno D, Petronio AS, Prendergast B, Eltchaninoff H, Vahanian A, Modine T, Lancellotti P, Sondergaard L, Ludman PF, Tamburino C, et al. Standardized definitions of structural deterioration and valve failure in assessing long-term durability of transcatheter and surgical aortic bioprosthetic valves: a consensus statement from the European Association of Percutaneous Cardiovascular Interventions (EAPCI) endorsed by the European Society of Cardiology (ESC) and the European Association for Cardio-Thoracic Surgery (EACTS). *Eur Heart J*. 2017;38:3382–3390. doi: [10.1093/eurheartj/ehx303](https://doi.org/10.1093/eurheartj/ehx303)
7. Dvir D, Bourguignon T, Otto CM, Hahn RT, Rosenhek R, Webb JG, Treede H, Sarano ME, Feldman T, Wijeyundera HC, et al. Standardized definition of structural valve degeneration for surgical and transcatheter bioprosthetic aortic valves. *Circulation*. 2018;137:388–399. doi: [10.1161/CIRCULATIONAHA.117.030729](https://doi.org/10.1161/CIRCULATIONAHA.117.030729)
8. Pibarot P, Dumesnil JG. Prosthetic heart valves: selection of the optimal prosthesis and long-term management. *Circulation*. 2009;119:1034–1048. doi: [10.1161/CIRCULATIONAHA.108.778886](https://doi.org/10.1161/CIRCULATIONAHA.108.778886)
9. Manji RA, Lee W, Cooper DKC. Xenograft bioprosthetic heart valves: past, present and future. *Int J Surg*. 2015;23:280–284. doi: [10.1016/j.ijsu.2015.07.009](https://doi.org/10.1016/j.ijsu.2015.07.009)
10. Tam H, Zhang W, Infante D, Parchment N, Sacks M, Vyavahare N. Fixation of bovine pericardium-based tissue biomaterial with irreversible chemistry improves biochemical and biomechanical properties. *J Cardiovasc Transl Res*. 2017;10:194–205. doi: [10.1007/s12265-017-9733-5](https://doi.org/10.1007/s12265-017-9733-5)
11. Kostyunin A, Yuzhalin A, Rezvova M, Ovcharenko E, Glushkova T, Kutikhin A. Degeneration of bioprosthetic heart valves: update 2020. *J Am Heart Assoc*. 2020;9:e018506. doi: [10.1161/JAHA.120.018506](https://doi.org/10.1161/JAHA.120.018506)
12. Barbarash L, Rutkovskaya N, Barbarash O, Odarenko Y, Stasev A, Uchasova E. Prosthetic heart valve selection in women of childbearing age with acquired heart disease: a case report. *J Med Case Rep*. 2016;10:51. doi: [10.1186/s13256-016-0821-y](https://doi.org/10.1186/s13256-016-0821-y)
13. Barbarash O, Rutkovskaya N, Hryachkova O, Gruzdeva O, Uchasova E, Ponasenko A, Kondyukova N, Odarenko Y, Barbarash L. Impact of recipient-related factors on structural dysfunction of xenoaortic bioprosthetic heart valves. *Patient Prefer Adherence*. 2015;9:389–399. doi: [10.2147/PPA.S76001](https://doi.org/10.2147/PPA.S76001)
14. Karaskov A, Sharifulin R, Zheleznev S, Demin I, Lenko E, Bogachev-Prokophiev A. Results of the Ross procedure in adults: a single-Centre experience of 741 operations. *Eur J Cardiothorac Surg*. 2016;49:e97–e104. doi: [10.1093/ejcts/ezw047](https://doi.org/10.1093/ejcts/ezw047)
15. Nichay NR, Zhuravleva IY, Kulyabin YY, Zubritskiy AV, Voitov AV, Soynov IA, Gorbatykh AV, Bogachev-Prokophiev AV, Karaskov AM. Diepoxy-versus glutaraldehyde-treated xenografts: outcomes of right ventricular outflow tract reconstruction in children. *World J Pediatr Congenit Heart Surg*. 2020;11:56–64. doi: [10.1177/2150135119885900](https://doi.org/10.1177/2150135119885900)
16. Pibarot P, Dumesnil JG. Improving assessment of aortic stenosis. *J Am Coll Cardiol*. 2012;60:169–180. doi: [10.1016/j.jacc.2011.11.078](https://doi.org/10.1016/j.jacc.2011.11.078)
17. Akahori H, Tsujino T, Masuyama T, Ishihara M. Mechanisms of aortic stenosis. *J Cardiol*. 2018;71:215–220. doi: [10.1016/j.jcc.2017.11.007](https://doi.org/10.1016/j.jcc.2017.11.007)
18. Manno G, Bentivegna R, Morreale P, Nobile D, Santangelo A, Novo S, Novo G. Chronic inflammation: a key role in degeneration of bicuspid aortic valve. *J Mol Cell Cardiol*. 2019;130:59–64. doi: [10.1016/j.yjmcc.2019.03.013](https://doi.org/10.1016/j.yjmcc.2019.03.013)
19. Katsi V, Magkas N, Antonopoulos A, Trantalos G, Toutouzas K, Tousoulis D. Aortic valve: anatomy and structure and the role of vasculature in the degenerative process. *Acta Cardiol*. 2021;76:335–348. doi: [10.1080/00015385.2020.1746053](https://doi.org/10.1080/00015385.2020.1746053)
20. Sellers SL, Gulsin GS, Zaminski D, Bing R, Latib A, Sathananthan J, Pibarot P, Bouchareb R. Platelets: implications in aortic valve stenosis and bioprosthetic valve dysfunction from pathophysiology to clinical care. *JACC Basic Transl Sci*. 2021;6:1007–1020. doi: [10.1016/j.jacbs.2021.07.008](https://doi.org/10.1016/j.jacbs.2021.07.008)
21. Habib G, Lancellotti P, Antunes MJ, Bongiorni MG, Casalta JP, Del Zotti F, Dulgheru R, El Khoury G, Erba PA, Lung B, et al. ESC guidelines for the management of infective endocarditis: the task force for the management of infective endocarditis of the European Society of Cardiology (ESC), endorsed by: European Association for Cardio-Thoracic Surgery (EACTS), the European Association of Nuclear Medicine (EANM). *Eur Heart J*. 2015;36:3075–3128. doi: [10.1093/eurheartj/ehv319](https://doi.org/10.1093/eurheartj/ehv319)
22. Mukhamdiyarov RA, Bogdanov LA, Glushkova TV, Shishkova DK, Kostyunin AE, Koshelev VA, Shabaev AR, Frolov AV, Stasev AN, Lyapin AA, et al. Embedding and backscattered scanning electron microscopy: a detailed protocol for the whole-specimen, high-resolution analysis of cardiovascular tissues. *Front Cardiovasc Med*. 2021;8:739549. doi: [10.3389/fcvm.2021.739549](https://doi.org/10.3389/fcvm.2021.739549)
23. Kostyunin A, Glushkova T, Stasev A, Mukhamdiyarov R, Velikanova E, Bogdanov L, Sinititskaya A, Asanov M, Ovcharenko E, Barbarash L, et al. Early postoperative immunothrombosis of bioprosthetic mitral valve and left atrium: a case report. *Int J Mol Sci*. 2022;23:6736. doi: [10.3390/ijms23126736](https://doi.org/10.3390/ijms23126736)
24. Ovcharenko EA, Klyshnikov KU, Yuzhalin AE, Savrasov GV, Glushkova TV, Vasukov GU, Nushtaev DV, Kudryavtseva YA, Barbarash LS. Comparison of xenopericardial patches of different origin and type of fixation implemented for TAVI. *Int J Biomed Eng Technol*. 2017;25:44–59. doi: [10.1504/IBET.2017.086551](https://doi.org/10.1504/IBET.2017.086551)
25. Gallili U. Anti-gal: an abundant human natural antibody of multiple pathogeneses and clinical benefits. *Immunology*. 2013;140:1–11. doi: [10.1111/imm.12110](https://doi.org/10.1111/imm.12110)
26. Salama A, Evanno G, Harb J, Soullou JP. Potential deleterious role of anti-Neu5Gc antibodies in xenotransplantation. *Xenotransplantation*. 2015;22:85–94. doi: [10.1111/xen.12142](https://doi.org/10.1111/xen.12142)
27. Konakci KZ, Bohle B, Blumer R, Hoetzenecker W, Roth G, Moser B, Boltz-Nitulescu G, Gorlitzer M, Klepetko W, Wolner E, et al. Alpha-gal on bioprostheses: xenograft immune response in cardiac surgery. *Eur J Clin Invest*. 2005;35:17–23. doi: [10.1111/j.1365-2362.2005.01441.x](https://doi.org/10.1111/j.1365-2362.2005.01441.x)
28. Lee W, Long C, Ramsoondar J, Ayares D, Cooper DK, Manji RA, Hara H. Human antibody recognition of xenogeneic antigens (NeuGc and gal) on porcine heart valves: could genetically modified pig heart valves reduce structural valve deterioration? *Xenotransplantation*. 2016;23:370–380. doi: [10.1111/xen.12254](https://doi.org/10.1111/xen.12254)
29. Vyavahare N, Ogle M, Schoen FJ, Zand R, Gloeckner DC, Sacks M, Levy RJ. Mechanisms of bioprosthetic heart valve failure: fatigue causes collagen denaturation and glycosaminoglycan loss. *J Biomed Mater Res*. 1999;46:44–50. doi: [10.1002/\(sici\)1097-4636\(199907\)46:1<44::aid-jbm5>3.0.co;2-d](https://doi.org/10.1002/(sici)1097-4636(199907)46:1<44::aid-jbm5>3.0.co;2-d)
30. Ellsmere JC, Khanna RA, Lee JM. Mechanical loading of bovine pericardium accelerates enzymatic degradation. *Biomaterials*. 1999;20:1143–1150. doi: [10.1016/s0142-9612\(99\)00013-7](https://doi.org/10.1016/s0142-9612(99)00013-7)
31. Margueratt SD, Lee JM. Stress state during fixation determines susceptibility to fatigue-linked biodegradation in bioprosthetic heart valve materials. *Biomed Sci Instrum*. 2002;38:145–150.
32. Sun W, Sacks M, Fulchiero G, Lovekamp J, Vyavahare N, Scott M. Response of heterograft heart valve biomaterials to moderate cyclic loading. *J Biomed Mater Res A*. 2004;69:658–669. doi: [10.1002/jbm.a.30031](https://doi.org/10.1002/jbm.a.30031)
33. Whelan A, Duffy J, Gaul RT, O'Reilly D, Nolan DR, Gunning P, Lally C, Murphy BP. Collagen fibre orientation and dispersion govern ultimate tensile strength, stiffness and the fatigue performance of bovine pericardium. *J Mech Behav Biomed Mater*. 2019;90:54–60. doi: [10.1016/j.jmbbm.2018.09.038](https://doi.org/10.1016/j.jmbbm.2018.09.038)
34. Sacks MS. A review on the biomechanical effects of fatigue on the porcine bioprosthetic heart valve. *J Long Term Eff Med Implants*. 2017;27:181–197. doi: [10.1615/JLongTermEffMedImplants.v27.i2-4.60](https://doi.org/10.1615/JLongTermEffMedImplants.v27.i2-4.60)
35. Friebe VM, Mikulis B, Kole S, Ruffing CS, Sacks MS, Vyavahare NR. Neomycin enhances extracellular matrix stability of glutaraldehyde crosslinked bioprosthetic heart valves. *J Biomed Mater Res B Appl Biomater*. 2011;99:217–229. doi: [10.1002/jbm.b.31889](https://doi.org/10.1002/jbm.b.31889)
36. Raghavan D, Starcher BC, Vyavahare NR. Neomycin binding preserves extracellular matrix in bioprosthetic heart valves during in vitro cyclic fatigue and storage. *Acta Biomater*. 2009;5:983–992. doi: [10.1016/j.actbio.2008.11.004](https://doi.org/10.1016/j.actbio.2008.11.004)
37. Simionescu DT, Lovekamp JJ, Vyavahare NR. Extracellular matrix degrading enzymes are active in porcine stentless aortic bioprosthetic heart valves. *J Biomed Mater Res A*. 2003;66:755–763. doi: [10.1002/jbm.a.10066](https://doi.org/10.1002/jbm.a.10066)
38. Zhuravleva IY, Karpova EV, Oparina LA, Poveschenko OV, Surovtseva MA, Titov AT, Ksenofontov AL, Vasilieva MB, Kuznetsova EV, Bogachev-Prokophiev AV, et al. Cross-linking method using pentaepoxide for improving bovine and porcine bioprosthetic pericardia: a multiparametric assessment study. *Mater Sci Eng C Mater Biol Appl*. 2021;118:111473. doi: [10.1016/j.msec.2020.111473](https://doi.org/10.1016/j.msec.2020.111473)
39. Christian AJ, Lin H, Alferiev IS, Connolly JM, Ferrari G, Hazen SL, Ischiropoulos H, Levy RJ. The susceptibility of bioprosthetic heart valve leaflets to oxidation. *Biomaterials*. 2014;35:2097–2102. doi: [10.1016/j.biomaterials.2013.11.045](https://doi.org/10.1016/j.biomaterials.2013.11.045)
40. Lee S, Levy RJ, Christian AJ, Hazen SL, Frick NE, Lai EK, Grau JB, Bavaria JE, Ferrari G. Calcification and oxidative modifications

-
- are associated with progressive bioprosthetic heart valve dysfunction. *J Am Heart Assoc.* 2017;6:e005648. doi: [10.1161/JAHA.117.005648](https://doi.org/10.1161/JAHA.117.005648)
41. Lovekamp JJ, Simionescu DT, Mercuri JJ, Zubiato B, Sacks MS, Vyavahare NR. Stability and function of glycosaminoglycans in porcine bioprosthetic heart valves. *Biomaterials.* 2006;27:1507–1518. doi: [10.1016/j.biomaterials.2005.08.003](https://doi.org/10.1016/j.biomaterials.2005.08.003)
 42. Simionescu DT, Lovekamp JJ, Vyavahare NR. Glycosaminoglycan-degrading enzymes in porcine aortic heart valves: implications for bioprosthetic heart valve degeneration. *J Heart Valve Dis.* 2003;12:217–225.
 43. Kostyunin A, Mukhamadiyarov R, Glushkova T, Bogdanov L, Shishkova D, Osyayev N, Ovcharenko E, Kutikhin A. Ultrastructural pathology of atherosclerosis, calcific aortic valve disease, and bioprosthetic heart valve degeneration: commonalities and differences. *Int J Mol Sci.* 2020;21:7434. doi: [10.3390/ijms21207434](https://doi.org/10.3390/ijms21207434)
 44. Ding K, Zheng C, Huang X, Zhang S, Li M, Lei Y, Wang Y. A PEGylation method of fabricating bioprosthetic heart valves based on glutaraldehyde and 2-amino-4-pentenoic acid co-crosslinking with improved antithrombogenicity and cytocompatibility. *Acta Biomater.* 2022;144:279–291. doi: [10.1016/j.actbio.2022.03.026](https://doi.org/10.1016/j.actbio.2022.03.026)

Supplemental Material

Data S1.

Supplemental Methods

Patients and valves

Here we interrogated 11 EGDE-treated BHVs (KemCor, PeriCor or UniLine, NeoCor) removed during the repeated heart valve replacement because of their failure. KemCor and PeriCor are xenoaortic (porcine) BHVs (XAP-BHVs, n = 5) while UniLine is a xenopericardial (bovine) BHV (XPB-BHVs, n = 6). One XPB-BHV was excised because of immunothrombosis 2 days postimplantation and this case was described earlier.¹⁸ Upon the excision, BHVs were immersed into the physiological saline and transferred to the laboratory for the gross examination. Following the separation of the leaflets from the frame, degenerated valve segments were excised, snap-frozen in the optimal cutting temperature medium (Tissue-Tek, 4583, Sakura), and cut on a cryostat (Microm HM 525, Thermo Fisher Scientific). Serial sections (6 µm thickness) were prepared from the center of the leaflets (from their base to the free margin), frame sheath, and any other segments with perforations, tearing or calcification (Figure S1). Remaining leaflet segments were employed for the total protein extraction, DNA extraction, and whole-specimen electron microscopy (EM-BSEM method¹⁷). In the same manner, we investigated 5 AVs excised during the primary heart valve replacement due to CAVD.

The investigation was carried out in accordance with the Good Clinical Practice and the Declaration of Helsinki. The study protocol was approved by the Local Ethical Committee of Research Institute for Complex Issues of Cardiovascular Diseases (Protocol No. 20190606, date of approval: 06/06/2019). All patients provided a written informed consent after receiving a full explanation of the study. Criteria of inclusion were: 1) replacement of EGDE-treated BHV due

to its failure (or replacement of the AV because of CAVD); 2) absence of any clinical and echocardiographic signs of infective endocarditis as well as negative blood inoculation before the surgery according to the respective European Society of Cardiology guidelines; 3) signed written informed consent to participate in the study. Criteria of exclusion were: 1) any gross signs of prosthetic valve endocarditis or any positive blood inoculation upon the BHV or AV replacement; 2) withdrawal of the written informed consent to participate in the study.

Sex distribution and prevalence of comorbid conditions, i.e., hyper/dyslipidaemia, overweight/obesity, diabetes mellitus, chronic kidney disease, arterial hypertension, and functional class of chronic heart failure did not differ significantly between the recipients of XAP-BHVs and XPB-BHVs (Table S1). Clinico- and histopathological features of BHV types and calcified AVs are documented in Table S2. XAP-BHVs had longer lifespan than XPB-BHVs. Indications for the repeated heart valve replacement were valvular stenosis (n = 2), insufficiency (n = 6), or their combination (n = 3). Gross examination identified SVD (defined as perforations, tearing or calcification of the leaflets) as the primary cause of BHV failure in 10 of 11 removed valves. AVs were strongly thickened and heavily calcified, suffering from the impaired leaflet motion. In all (5/5) cases, the reason for the primary heart valve replacement was calcific aortic stenosis.

Total protein extraction

For the protein extraction, we used the part of the leaflets from their base to the free margin. To extract the total protein from the BHVs or AVs, tissues were homogenised (FastPrep-24 5G, MP Biomedicals; Lysing Matrix S Tubes, 116925050-CF, MP Biomedicals) in T-PER buffer (78510, Thermo Fisher Scientific) supplied with Halt protease and phosphatase inhibitor cocktail (78444, Thermo Fisher Scientific) according to the manufacturer's protocol. Upon the initial centrifugation at $14\,000 \times g$ (Microfuge 20R, Beckman Coulter) for 10 minutes,

supernatant was additionally centrifuged at $200\,000 \times g$ (Optima MAX-XP, Beckman Coulter) for 30 minutes to sediment insoluble ECM proteins. Quantification of total protein was conducted using BCA Protein Assay Kit (23227, Thermo Fisher Scientific) and Multiskan Sky microplate spectrophotometer (Thermo Fisher Scientific) in accordance with the manufacturer's protocol.

Proteomic profiling

Upon the removal of T-PER Buffer by acetone precipitation (650501, Sigma-Aldrich), protein pellet was resuspended in 8 mol/L urea (U5128, Sigma-Aldrich) diluted in 50 mmol/L ammonium bicarbonate (09830, Sigma-Aldrich). The protein concentration was measured by Qubit 4 fluorometer (Q33238, Thermo Fisher Scientific) with QuDye Protein Quantification Kit (25102, Lumiprobe) according to the manufacturer's protocol. Protein samples (10 μ g) were then incubated in 5 mmol/L dithiothreitol (D0632, Sigma-Aldrich) for 1 hour at 37°C with the subsequent incubation in 15 mmol/L iodoacetamide for 30 minutes in the dark at room temperature (I1149, Sigma-Aldrich). Next, the samples were diluted with 7 volumes of 50 mmol/L ammonium bicarbonate and incubated for 16 hours at 37°C with 200 ng of trypsin (1:50 trypsin:protein ratio; VA9000, Promega). The peptides were then frozen at -80°C for 1 hour, dried in Labconco CentriVap Centrifugal Concentrator (Labconco) for 3 hours, dissolved in 0.1% formic acid (33015, Sigma-Aldrich; 1153334000, Sigma-Aldrich) and desalted with C18 spin tips (84850, Thermo Fisher Scientific) according to the manufacturer's protocol. Desalted peptides were dried in Labconco CentriVap Centrifugal Concentrator (Labconco) for 2 hours and finally dissolved in 20 μ L 0.1% formic acid for the further LC-MS/MS analysis. One of the XPB-BHV has not been profiled as it failed due to immunothrombosis rather than SVD; yet, its sections and protein lysate were used as a positive control for the antibodies on

immunohistochemistry and Western blotting. Previously, this clinical case has been described in detail.¹⁸

Approximately 500 ng of peptides were used for shotgun proteomics analysis by ultra-high performance liquid chromatography-tandem mass spectrometry (UHPLC-MS/MS) with ion mobility in TimsToF Pro mass spectrometer with nanoElute UHPLC system (Bruker Daltonics). UHPLC was performed in the two-column separation mode with Acclaim PepMap 5 mm Trap Cartridge (Thermo Fisher Scientific) and Bruker Fifteen separation column (C18 ReproSil AQ, 150 mm × 0.75 mm, 1.9 μm, 120 Å; Bruker Daltonics) in a gradient mode with 400 nL/min flow rate and 40°C. Phase A was water/0.1% formic acid, phase B was acetonitrile/0.1% formic acid (1000291000, Sigma-Aldrich). The gradient was from 2% to 30% phase B for 42 min, then to 95% phase B for 6 min with subsequent washing with 95% phase B for 6 min. Before each sample, trap and separation columns were equilibrated with 10 and 4 column volumes, respectively. CaptiveSpray ion source was used for electrospray ionization with 1600 V of capillary voltage, 3 L/min N₂ flow, and 180°C source temperature. The mass spectrometry acquisition was performed in DDA-PASEF mode with 0.5 s cycle in positive polarity with the fragmentation of ions with at least two charges in m/z range from 100 to 1700 and ion mobility range from 0.85 to 1.30 1/K0.

Protein identification was performed in PEAKS Studio Xpro software (a license granted to St. Petersburg State University; Bioinformatics Solutions Inc., Waterloo, ON, Canada) using human protein SwissProt database (<https://www.uniprot.org/>; accessed on 20 July 2022; organism: Human [9606]; uploaded on 2 March 2021; 20,394 sequences) and protein contaminants database CRAP (version of 4 March 2019). The search parameters were: parent mass error tolerance 10 ppm and fragment mass error tolerance 0.05 ppm, protein and peptide FDR < 1% and 0.1% respectively, two possible missed cleavage sites, proteins with ≥ 2 unique peptides. Cysteine carbamidomethylation was set as fixed modification. Methionine oxidation,

N-terminal acetylation, asparagine and glutamine deamidation were set as variable modifications.

The mass spectrometry proteomics data have been deposited to the ProteomeXchange Consortium via the PRIDE partner repository with the dataset identifiers PXD035113 and 10.6019/PXD035113. Label-free quantification by peak area under the curve and spectral counts was used for the further analysis in R (version 3.6.1; R Core Team, 2019). All proteins presented in ≥ 3 of 5 biological replicates were identified and the groups were compared by “VennDiagram” package and drawing of Venn diagram. The proteins with NA in $> 25\%$ of samples were removed and imputation of missed values by k-nearest neighbors was performed by the “impute” package. Then, log-transformation and quantile normalization with further analysis of differential expression by “limma” package were conducted. Finally, we carried out clusterisation of samples by sparse partial least squares discriminant analysis in the package “MixOmics”. “ggplot2” and “EnhancedVolcano” packages were used for visualization. Reproducible code for data analysis is available from <https://github.com/ArseniyLobov/bioprosthetic-valve-failure-proteomics> (accessed on 20 July 2022). Unique proteins were defined as those presented in ≥ 8 BHVs and ≤ 1 AV or those presented in ≥ 3 XAP-BHVs and ≥ 3 XPB-BHVs while not being presented in the AVs.

Western blotting

Semi-quantitative measurement of 35 proteases and 32 specific inhibitors in the BHV or AV lysate was performed by dot blotting (130 μg total protein per sample) employing a respective kit (R&D, ARY025). Chemiluminescent detection was carried out using a C-DiGit blot scanner (LI-COR Biosciences) in a high-sensitivity mode (12-minute scanning). Expression of myeloperoxidase (MPO) and neutrophil elastase (NE/ELA2) has been defined by Western blotting. Equal amounts of protein (25 μg per sample) were mixed with NuPAGE

LDS sample buffer (NP0007, Thermo Fisher Scientific) in a 4:1 ratio and NuPAGE sample reducing agent (NP0009, Thermo Fisher Scientific) at a 10:1 ratio, and then loaded on a 1.5 mm NuPAGE 4–12% Bis-Tris protein gel (NP0335BOX, Thermo Fisher Scientific). The 1:1 mixture of Novex Sharp pre-stained protein standard (LC5800, Thermo Fisher Scientific) and MagicMark XP Western protein standard (LC5602, Thermo Fisher Scientific) was loaded as a molecular weight marker. Proteins were separated by a sodium dodecyl sulphate-polyacrylamide gel electrophoresis at 150 V for 90 min. Protein transfer was performed using polyvinylidene difluoride (PVDF) transfer stacks (IB24001, Thermo Fisher Scientific) and iBlot 2 Gel Transfer Device (Thermo Fisher Scientific) according to the manufacturer's protocols.

Blots were probed with rabbit antibodies to MPO (ab208670, Abcam, 1:1000 dilution) or mouse antibodies to NE/ELA2 (MAB91671-100, Novus Biologicals, 1:1000). Horseradish-peroxidase-conjugated goat anti-rabbit (7074, Cell Signaling Technology) or goat anti-mouse secondary antibodies (AP130P, Sigma-Aldrich) were used at 1:200 and 1:1000 dilution, respectively. Incubation with the antibodies was performed using iBind Flex Solution Kit (SLF2020, Thermo Fisher Scientific), iBind Flex Cards (SLF2010, Thermo Fisher Scientific) and Bind Flex Western Device (Thermo Fisher Scientific, Waltham, MA, USA) according to the manufacturer's protocols. Chemiluminescent detection was performed using SuperSignal West Pico PLUS chemiluminescent substrate (34580, Thermo Fisher Scientific) and a C-DiGit blot scanner (LI-COR Biosciences) in a high-sensitivity mode (12-min scanning). Densitometry was performed using ImageJ software (National Institutes of Health, Bethesda, MD, USA).

Microbial identification

For the DNA extraction, ≈ 5 mg fragments of BHVs and AVs were homogenised (FastPrep-24 5G, MP Biomedicals; Lysing Matrix D tubes, 116913050-CF, MP Biomedicals)

in the physiological saline according to the manufacturer's protocol. DNA isolation was conducted using a Tissue Nucleic Acid-Sorbent Kit (0232-2, Lytech, Russia) according to the manufacturer's protocol. Microbial identification was carried out by PCR using specific kits for *Streptococcus spp.* (01773-PB-OS-96, Lytech), *Staphylococcus spp.* (01757-PB-OS-96, Lytech), and *Enterobacter spp.* (01766-PB-OS-96, Lytech). Amplification was carried out using the CFX96 Touch Real-Time PCR Detection System (Bio-Rad Laboratories), Bio-Rad CFX Manager 3.1 Software, FAM (specific signal) and HEX (internal control) channels.

Histological, immunohistochemical, and immunofluorescence analysis

Cellular infiltration and ECM degradation were assessed by Russell-Movat's pentachrome staining (ab245884, Abcam) and haematoxylin and eosin staining (05-06004, Bio-Optica) while lipid deposition and calcification were analysed by Oil Red O (ab150678, Abcam) and Alizarin Red S staining (ab142980, Abcam) according to the manufacturers' protocols. To evaluate the colocalisation of calcified deposits and host cells, sections stained with Alizarin Red S were counterstained with 4',6-diamidino-2-phenylindole (DAPI, 10 µg/mL, D9542, Sigma-Aldrich). Bacteria and fungi were detected by Gram staining (ab150672, Abcam) and periodic acid-Schiff (PAS) staining (ab245886, Abcam), respectively. Immune cell and MMP/TIMP profiling was performed after the fixation in 4% paraformaldehyde (P6148, Sigma-Aldrich) by immunohistochemical staining (Novolink Max Polymer Detection System, RE7280-K, Leica) according to the manufacturer's protocol using the antibodies to a pan-leukocyte marker CD45 (ab10558, Abcam, 1:4000 dilution), macrophage marker CD68 (ab955, Abcam, 1:1000), neutrophil markers myeloperoxidase (MPO, ab208670, Abcam, 1:8000) and NE/ELA2 (MAB91671-100, Novus Biologicals, 1:2000), T cell marker CD3 (ab16669, Abcam, 1:1000), B cell marker CD19 (MA5-32544, Invitrogen, 1:1000), MMP-1 (ab52631, Abcam, 1:1000), MMP-2 (ab92536, Abcam, 1:1000), MMP-9 (ab38898, Abcam,

1:1000), MMP-12 (ab52897, Abcam, 1:1000), TIMP-1 (ab211926, Abcam, 1:2000), and TIMP-2 (ab1828, Abcam, 1:2000). In a positive control case,¹⁸ thrombosis was confirmed by CD41 (ab134131, Abcam, 1:2000) and fibrin staining (NBP2-50407, Novus Biologicals, 1:1000). EGDE-treated porcine leaflets and bovine pericardium (NeoCor) which have not been used for the BHV fabrication were utilised as a negative control. For all immunohistochemical stainings, we prepared an additional negative control section without a primary or secondary antibody. Visualisation was conducted by light microscopy (AxioImager.A1, Carl Zeiss) employing AxioVision software (Carl Zeiss) in a blinded fashion by two independent pathologists.

The distribution of MMP-8 and MMP-9 within the BHVs and AVs and their colocalisation with NE/ELA2 was assessed by the immunofluorescence staining. Upon the air drying for 30 minutes, sections were fixed and permeabilised in ice-cold acetone for 10 minutes and were further incubated in 1% bovine serum albumin (A2153, Sigma–Aldrich) diluted in phosphate buffered saline (PBS, pH 7.4, P4417, Sigma-Aldrich) for 1 hour for the blocking of non-specific protein binding. Samples were then stained with unconjugated mouse primary antibody to NE/ELA2 (MAB91671-100, Novus Biologicals, 1:50) and rabbit primary antibody to either MMP-8 (ab53017, Abcam, 1:200) or MMP-9 (ab38898, Abcam, 1:100) and incubated at 4°C for 18 h. Slides were further treated with donkey anti-mouse Alexa Fluor 488-conjugated (ab150109, Abcam, 1:500) and donkey anti-rabbit Alexa Fluor 555-conjugated (ab150062, Abcam, 1:500) pre-adsorbed secondary antibodies and incubated for 1 hour at room temperature. Nuclei were counterstained with DAPI (10 µg/mL, D9542, Sigma–Aldrich) for 30 minutes. Between all steps excepting the protein block, washing was performed thrice with PBS. Coverslips were mounted with ProLong Gold Antifade (P36934, Thermo Fisher Scientific). Slides were examined by confocal laser scanning microscopy (LSM 700, Carl Zeiss) in a blinded fashion by two independent pathologists. Semi-quantitative image analysis

was carried out by ImageJ (National Institutes of Health). Colocalisation analysis (n = 10 images per group) was performed using the respective ImageJ (National Institutes of Health) plugins (Colocalisation Threshold and Coloc2). To evaluate the colocalisation, we calculated thresholded Mander's split colocalisation coefficient (the proportion of signal in each channel that is colocalised with the other channel) for red channel.

Whole-specimen backscattered scanning electron microscopy (EM-BSEM)

Sample preparation and EM-BSEM was performed as described in a recent paper by our group.¹⁷ Briefly, fragments of BHVs and AVs were fixed in two changes of 10% neutral phosphate-buffered formalin (HT501128, Sigma-Aldrich) for 24 hours at 4 °C, postfixed in 1% osmium tetroxide (OsO₄, 19110, Electron Microscopy Sciences) for 16 hours, stained in 2% osmium tetroxide for 40 hours, dehydrated in ascending ethanol series (50%, 60%, 70%, 80% and 95%, two changes per concentration, 15 minutes per change), stained in 2% alcoholic uranyl acetate (22400-2, Electron Microscopy Sciences) for 16 hours, dehydrated in isopropanol (2 hours) and acetone (2 hours), impregnated with an acetone : epoxy resin (Araldite 502, 13900, Electron Microscopy Sciences) mixture (1:1) for 16 hours and with epoxy resin for 24 hours, and were finally embedded into fresh epoxy resin at 60°C for 24 hours. Samples were then grinded and polished (TegraPol-11, Struers), and counterstained with Reynolds's lead citrate (17810, Electron Microscopy Sciences) for 7 minutes. After a washing in double distilled water, samples were sputter-coated (10 nm thickness) with carbon (EM ACE200, Leica Biosystems) and visualised by means of backscattered scanning electron microscopy at a 10 or 15 kV accelerating voltage (S-3400N, Hitachi).

Statistical analysis

Evaluation of cellular infiltration, lipid deposition, microbial invasion, ECM degradation and calcification was performed by a semi-quantitative score from 0 to 3 where 0 corresponded to the absence of the feature of interest and 3 corresponded to its highest amount. Statistical analysis was performed using GraphPad Prism 8 (GraphPad Software). For descriptive statistics, data are presented as median, 25th and 75th percentiles, and range. Two independent groups were compared by the Mann–Whitney U-test, whereas three or more groups were compared by Pearson’s chi-squared test (optionally with Yates’s correction for continuity), Fisher’s exact test, or by Kruskal–Wallis test with post hoc calculation of false discovery rate (FDR) by the two-stage linear step-up procedure of Benjamini, Krieger, and Yekutieli. *P* values, or *q* values if FDR was applied (*q* values are the name given to the adjusted *p* values found using an optimised FDR approach), ≤ 0.05 were regarded as statistically significant.

Table S1. Age, sex, and comorbid conditions of patients who underwent primary or repeated heart valve replacement.

Case	Age at primary or repeated valve replacement (years)	Sex	Hyper- or dyslipidemia	Overweight or obesity	Diabetes mellitus	Chronic kidney disease	Arterial hypertension	Chronic heart failure (NYHA class)
Xenoaortic (porcine) bioprosthetic heart valves								
1	58	Male	-	+	+	-	+	III
2	54	Male	-	+	-	-	+	IV
3	50	Male	+	-	+	+	-	IV
4	33	Female	-	+	-	-	+	II
5	55	Female	+	-	-	-	+	III
Xenopericardial (bovine) bioprosthetic heart valves								
6	69	Male	-	-	-	+	+	III
7	31	Female	-	+	-	-	+	II
8	61	Male	-	+	-	+	+	II
9	66	Female	-	-	+	-	+	IV
10	66	Female	-	+	+	-	+	IV
11*	72	Female	-	-	-	-	-	II
Native calcified aortic valves								
12	66	Male	-	+	+	-	+	II
13	68	Female	+	+	-	-	+	III
14	72	Female	+	+	+	+	+	II
15	68	Female	-	+	+	+	+	III
16	66	Male	+	+	+	+	+	III
<i>P_{XAP-XPB}</i>	0.13	0.53	0.11	0.99	0.99	0.49	0.29	0.99
<i>P_{XAP-AV}</i>	0.005	0.53	0.53	0.11	0.2	0.2	0.29	0.73

<i>P</i> _{XPB-AV}	0.2	0.99	0.04	0.11	0.2	0.53	0.99	0.99
<i>P</i> _{M-F(BHV)}	0.65	N/A	0.99	0.99	0.99	0.17	0.99	0.99

+ and - mean the presence and absence of the indicated feature. *P* values ≤ 0.05 are marked

bold. *P*_{M-F(BHV)} is the *P* value for the comparison between male and female BHV recipients.

*Case #11 has not been included into the statistical analysis because this BHV was excised 2 days postimplantation and was therefore used as an internal control.

NYHA – New York Heart Association, XAP-BHVs – xenoaortic porcine bioprosthetic heart valves, XPB-BHVs – xenopericardial bovine bioprosthetic heart valves, AVs – aortic valves,

M – male, F – female.

Table S2. Lifespan, causes of failure, and lesions in XAP-BHVs, XPB-BHVs, and calcified AVs.

Case	Lifespan, months	Clinical diagnosis		Gross examination				Histological analysis			
		Regurgitation	Stenosis	Leaflet tearing	Thrombosis	Pannus	Macrocalcification	ECM degradation	Cellular infiltration	Lipid deposition	Microcalcification
Xenoaortic (porcine) bioprosthetic heart valves											
1	143	+	-	+	-	-	1	2	3	2	1
2	169	+	-	+	-	+	1	1	1	2	1
3	221	+	-	+	-	+	1	1	3	3	1
4	162	+	-	+	-	+	2	2	3	1	1
5	184	+	+	-	-	+	1	1	2	2	2
Xenopericardial (bovine) bioprosthetic heart valves											
6	34	+	+	-	-	-	3	1	2	0	1
7	75	-	+	-	-	+	3	1	1	0	1
8	68	+	-	-	-	+	1	1	2	2	1
9	30	+	-	-	-	-	1	1	2	0	1
10	78	+	+	-	-	-	3	1	2	0	1
11*	0,07	-	+	-	+	-	0	0	0/3 [†]	0	0
Native calcified aortic valves											
12		-	+	-	-	-	3	1	N/A	1	2
13		-	+	-	-	-	3	1	N/A	1	2
14		-	+	-	-	-	3	1	N/A	2	1
15		-	+	-	-	-	3	2	N/A	2	2
16		-	+	-	-	-	3	1	N/A	2	1
<i>P_{XAP-XPB}</i>	0.008	0.29	0.20	0.01	0.99	0.20	0.11	0.40	0.16	0.03	0.51
<i>P_{XAP-AV}</i>	N/A	0.002	0.01	0.01	0.99	0.01	0.008	0.47	N/A	0.35	0.26

<i>P</i> _{XPB-AV}	N/A	0.01	0.11	0.99	0.99	0.11	0.14	0.47	N/A	0.07	0.12
<i>P</i> _{M-F(BHV)}	0.84	0.99	0.52	0.52	0.99	0.99	0.52	0.99	0.88	0.17	0.99

+ and - mean the presence and absence of the indicated feature. *P* values ≤ 0.05 are marked

bold. *P*_{M-F(BHV)} is the *P* value for the comparison between male and female BHV recipients.

0, 1, 2 and 3 represent points rendered according to the semi-quantitative score (Table S3).

*Case #11 has not been included into the statistical analysis because this BHV was excised 2 days postimplantation and was therefore used as an internal control.

†means localisation within the BHV-associated thrombotic masses.

XAP-BHVs – xenoaortic porcine bioprosthetic heart valves, XPB-BHVs – xenopericardial bovine bioprosthetic heart valves, AVs – aortic valves, ECM – extracellular matrix, N/A – not applicable, M – male, F – female.

Table S3. Description of the semi-quantitative score for the gross examination or histological analysis.

Score	Gross examination		Histological analysis		
	Macrocalcification	Extracellular matrix degradation	Cellular infiltration (for BHVs)	Lipid deposition	Microcalcification
0	None	None	None	None	None
1	A few small-sized calcium deposits, retained leaflet motion	Loosening of collagen fibers, small tears within the ECM (for BHVs) or mild leaflet thickening (for AVs)	Sparse cells on the leaflet surface	Single small-to-medium lipid droplets	Minor calcium deposits
2	Multiple, small-to-medium-sized calcium deposits, slightly impaired leaflet motion	Disorganisation and fragmentation of collagen fibers, single perforations, cavities and tears within the ECM (for BHVs) or moderate leaflet thickening (for AVs)	Multiple cells on the leaflet surface; cell migration into the prosthetic valve	Numerous small-to-medium lipid droplets, single large lipid droplets	Multiple calcium deposits
3	Large calcium deposits or total leaflet calcification, significantly impaired leaflet motion	Disintegration of collagen fibers, multiple perforations, cavities and tears within the ECM (for BHVs) or severe leaflet thickening (for AVs)	Multiple cells on the leaflet surface; cell invasion across the entire valve	Numerous large lipid droplets	Ubiquitous calcium deposits

ECM – extracellular matrix, BHVs – bioprosthetic heart valves, AVs – aortic valves.

Table S4. Semi-quantitative immune cell count and bacterial count in XAP-BHVs, XPB-BHVs, and calcified AVs.

Case	Leukocytes (CD45 ⁺)	Macrophages (CD68 ⁺) [‡]	Foam cells (Oil Red O ⁺)	Neutrophils (MPO ⁺)	T cells (CD3 ⁺)	B cells (CD19 ⁺)	Bacteria (Gram staining + + PCR detection)
Xenoaortic (porcine) bioprosthetic heart valves							
1	3	3	1	3	0	0	2 (<i>Streptococcus spp.</i>)
2	1	1	1	1	1	0	2 (N/D)
3	3	2	0	3	1	0	1 (N/D)
4	3	2	2	3	2	0	2 (N/D)
5	2	2	1	0	1	0	1 (<i>Streptococcus spp.</i>)
Xenopericardial (bovine) bioprosthetic heart valves							
6	2	2	0	2	0	0	0
7	1	1	0	2	0	0	2 (<i>Streptococcus spp.</i>)
8	2	2	0	1	1	0	2 (<i>Streptococcus spp.</i>)
9	2	1	0	2	2	0	2 (<i>Streptococcus spp.</i>)
10	2	2	0	2	1	1	1 (N/D)
11*	0/3 [†]	0	0	0/3 [†]	0	0	0 (N/D)
Native calcified aortic valves							
12	2	2	1	0	1	0	0
13	2	2	0	0	2	0	0
14	2	2	1	0	0	0	0
15	1	1	0	0	0	0	0
16	2	2	0	0	1	0	0
<i>P</i> _{XAP-XPB}	0.23	0.67	0.02	0.28	0.99	0.35	0.26
<i>P</i> _{XAP-AV}	0.23	0.67	0.17	0.009	0.99	0.99	0.007
<i>P</i> _{XPB-AV}	0.99	0.67	0.18	0.009	0.99	0.35	0.009
<i>P</i> _{M-F(BHV)}	0.88	0.64	0.99	0.81	0.40	0.99	0.99

P values ≤ 0.05 are marked bold. *P*_{M-F(BHV)} is the *P* value for the comparison between male and female BHV recipients.

0, 1, 2 and 3 represent points rendered according to the semi-quantitative score (Table S5).

*Case #11 has not been included into the statistical analysis because this BHV was excised 2 days postimplantation and was therefore used as an internal control.

†means localisation within the BHV-associated thrombotic masses

‡count of macrophages also included foam cells because the latter are exclusively of macrophage origin in BHVs.

XAP-BHVs – xenoaortic porcine bioprosthetic heart valves, XPB-BHVs – xenopericardial bovine bioprosthetic heart valves, AVs – aortic valves, CD – cluster of differentiation, MPO – myeloperoxidase, PCR – polymerase chain reaction, N/D – not defined, M – male, F – female.

Table S5. Description of the semi-quantitative score for the immune cell count and bacterial count.

Score	Immune cells						Bacteria
	Leukocytes (CD45 ⁺)	Macrophages (CD68 ⁺)	Foam cells (Oil Red O ⁺)	Neutrophils (MPO ⁺)	T cells (CD3 ⁺)	B cells (CD19 ⁺)	
0			None				None
1		A few cells mainly located beneath the surface					A few bacteria underneath the surface
2		Multiple but sparse cells located across the prosthetic or native valve					Bacterial foci, mainly located below the surface
3		Total cellular infiltration					N/A

CD – cluster of differentiation, MPO – myeloperoxidase.

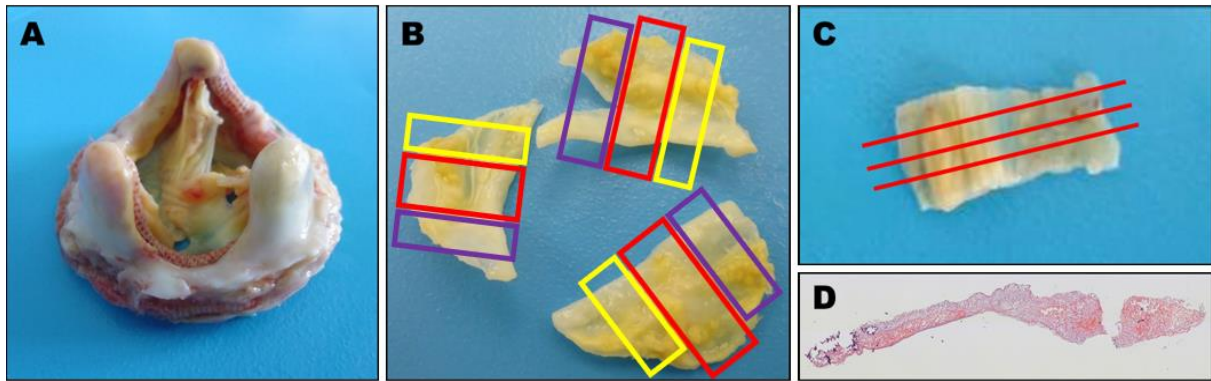


Figure S1. Selection of the regions of interest in EGDE-treated BHVs. **A.** Representative XAP-BHV removed from the mitral position. **B.** Representative BHV leaflets separated from the frame. Demarcated regions have been excised for the proteomic profiling, dot blotting screening, Western blotting, and PCR (yellow colour), histological and immunohistochemical staining (red colour), and whole-specimen backscattered scanning electron microscopy (EM-BSEM, purple colour). **C.** Center of the leaflet selected for the sectioning, representative segment (lines indicate the direction of sectioning). **D.** Representative section stained with haematoxylin and eosin. EGDE – ethylene glycol diglycidyl ether, XAP-BHVs – xenoaortic porcine bioprosthetic heart valves, PCR – polymerase chain reaction, EM-BSEM – embedding and backscattered scanning electron microscopy.

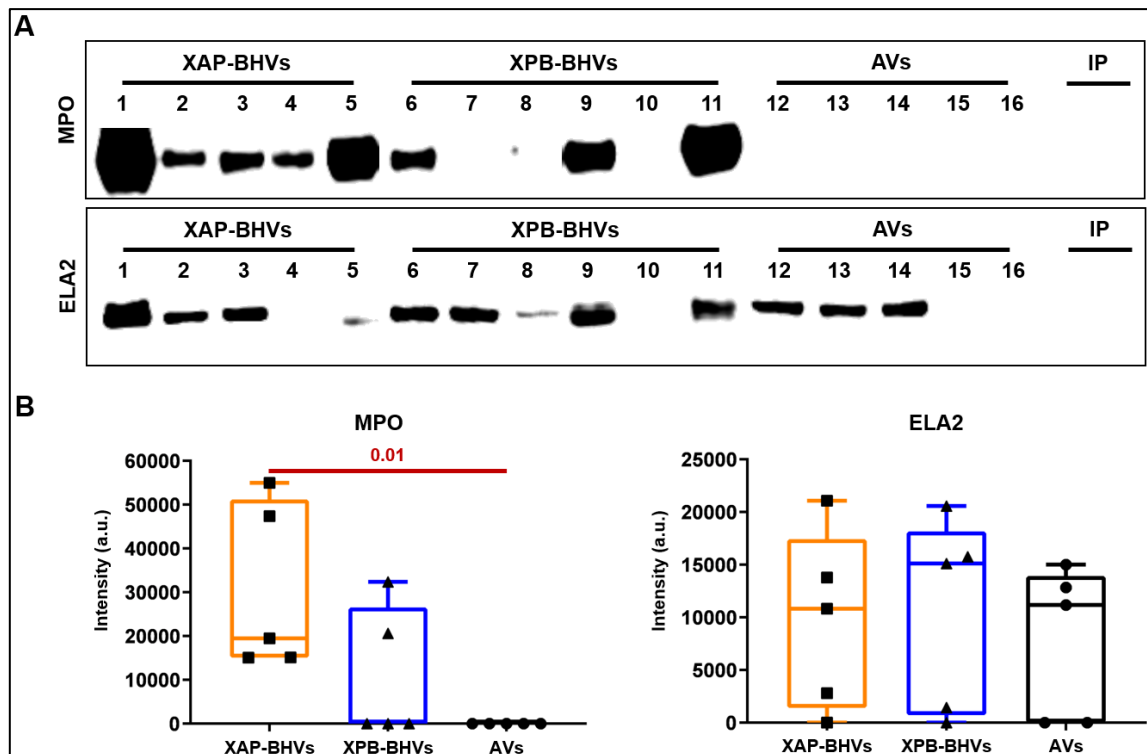


Figure S2. Determination of neutrophil markers (MPO and NE/ELA2) in XAP-BHVs, XPB-BHVs, and calcified AVs by Western blotting. **A.** Western blotting images, case numbers are indicated above. Case #11 (the XPB-BHV from the patient who died because of prosthetic immunothrombosis) represent a positive control for the neutrophil proteins. Intact bovine pericardium (IP) which has not been used for the BHV fabrication was used as a negative control. **B.** Densitometry of the images indicated in A (ImageJ). Case #11 was not taken into statistical analysis. Box-and-whisker plot combined with univariate scatterplot, center lines indicate median, boxes bounds indicate 25th–75th percentiles, whiskers indicate range. Each dot reflects a densitometry measurement from one prosthetic or native valve. Kruskal–Wallis test with post hoc false discovery rate (FDR) adjustment for multiple comparisons by two-stage linear step-up procedure of Benjamini, Krieger and Yekutieli. Statistically significant, FDR-corrected q values are provided above boxes. MPO – myeloperoxidase, NE/ELA2 – neutrophil elastase, XAP-BHVs – xenoaortic porcine bioprosthetic heart valves, XPB-BHVs – xenopericardial bovine bioprosthetic heart valves, AVs – aortic valves, IP – intact pericardium, FDR – false discovery rate.

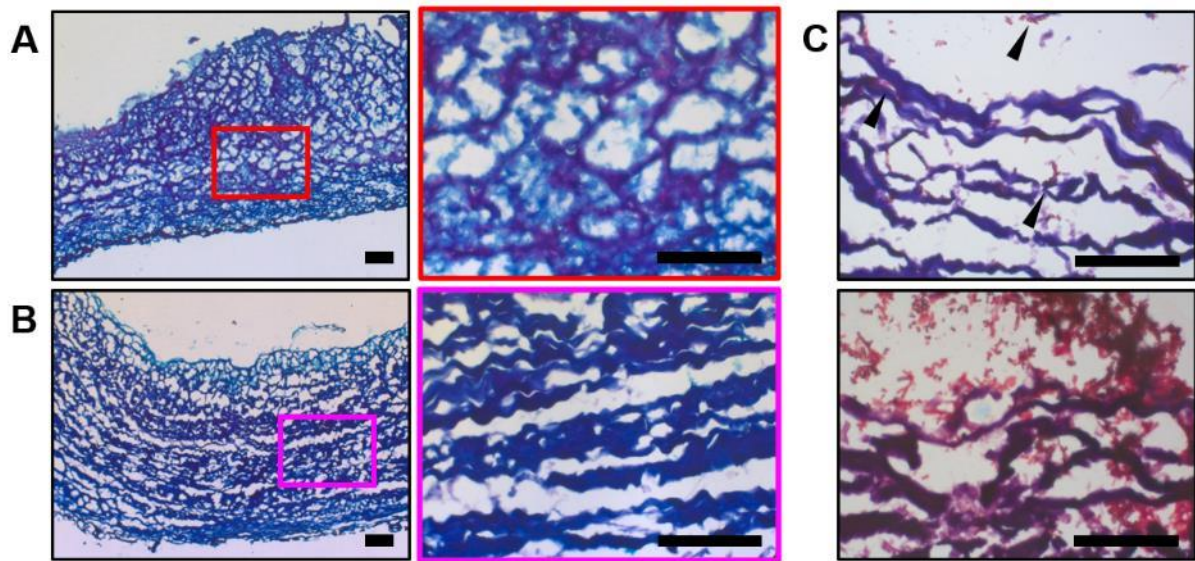


Figure S3. XAP-BHVs and XPB-BHVs are not contaminated by the fungi. **A.** XAP-BHVs. **B.** XPB-BHVs. For A and B: images to the right are close-ups of those to the left (demarcated by red or purple contour). Magnification: x100 (left) and x400 (right). **C.** Molds cultured on the intentionally contaminated non-implanted bovine pericardium (positive control, indicated by black arrows). Magnification: x400. For A–C: periodic acid-Schiff staining, representative images, scale bars: 100 μm . XAP-BHVs – xenoaortic porcine bioprosthetic heart valves, XPB-BHVs – xenopericardial bovine bioprosthetic heart valves.

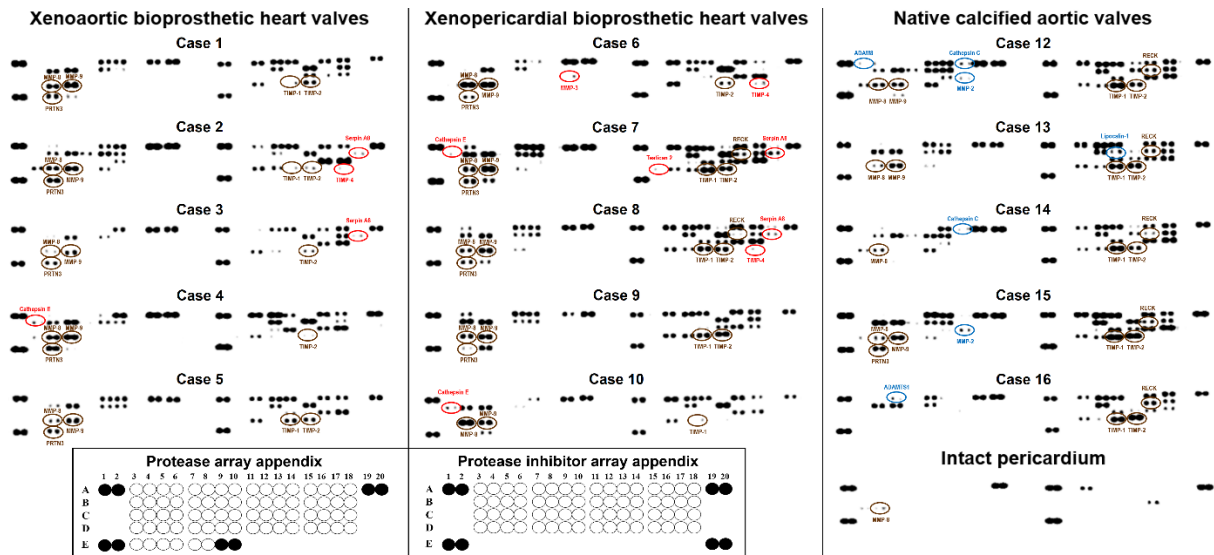


Figure S4. Profiling of XAP-BHVs, XPB-BHVs and calcified AVs for proteases/protease inhibitors. Note the overexpression of proteases (PRTN3, MMP-8, MMP-9) in BHVs and their depletion of protease inhibitors (TIMP-1 and TIMP-2). Proteases and protease inhibitors unique for BHVs and AVs are circled red and blue, respectively. PRTN3, MMP-8, MMP-9, TIMP-1, TIMP-2, and RECK are circled brown.

Keys for proteases: A3/4:ADAM8; A5/6:ADAM9; A7/8:ADAMTS1; A11/12:cathepsin A; A13/14:cathepsin B; A15/16:cathepsin C; A17/18:cathepsin D; B3/4:cathepsin E; B5/6:cathepsin L; B7/8:cathepsin S; B9/10:cathepsin V; B11/12:cathepsin X/Z/P; B13/14:DPP-4/CD26; C13/14:MMP-1; C15/16:MMP-2; C17/18:MMP-3; D3/4:MMP-7; D5/6:MMP-8; D7/8:MMP-9; D11/12:MMP-12; E5/6:myeloblastin (proteinase 3/PRTN3); E7/8:urokinase; A1/2/19/20, E1/2:reference spots; E9/10:negative control.

Keys for protease inhibitors: A5/6:cystatin A; A7/8:cystatin B; A9/10:cystatin C; A11/12:cystatin E/M; A13/14:EMMPRIN/CD147; A15/16:fetuin B; A17/18:HAI-1; B7/8:latexin; B9/10:lipocalin-1; B11/12:lipocalin-2; B13/14:RECK; B15/16:serpin A5; B17/18:serpin A8; C7/8:serpin B5; C9/10:serpin B6; C11/12:serpin B8; C13/14:serpin E1; C15/16:serpin F1; D3/4:testican-2; D5/6:TFPI; D7/8:TFPI-2; D9/10:TIMP-1; D11/12:TIMP-2; D15/16:TIMP-4; A1/2/19/20, E1/2:reference spots; E19/20:negative control.

XAP-BHVs – xenoaortic porcine bioprosthetic heart valves, XPB-BHVs – xenopericardial bovine bioprosthetic heart valves, AVs – aortic valves, PRTN3 – proteinase 3, MMP – matrix metalloproteinase, TIMP – tissue inhibitor of metalloproteinases, RECK – Reversion-inducing-cysteine-rich protein with kazal motifs, ADAM – a disintegrin and metalloproteinase, ADAMTS – a disintegrin and metalloproteinase with thrombospondin motifs, DPP – dipeptidyl peptidase, CD – cluster of differentiation, EMMPRIN – extracellular matrix metalloproteinase inducer, HAI – hepatocyte growth factor activator inhibitor-1, TFPI – tissue factor pathway inhibitor.

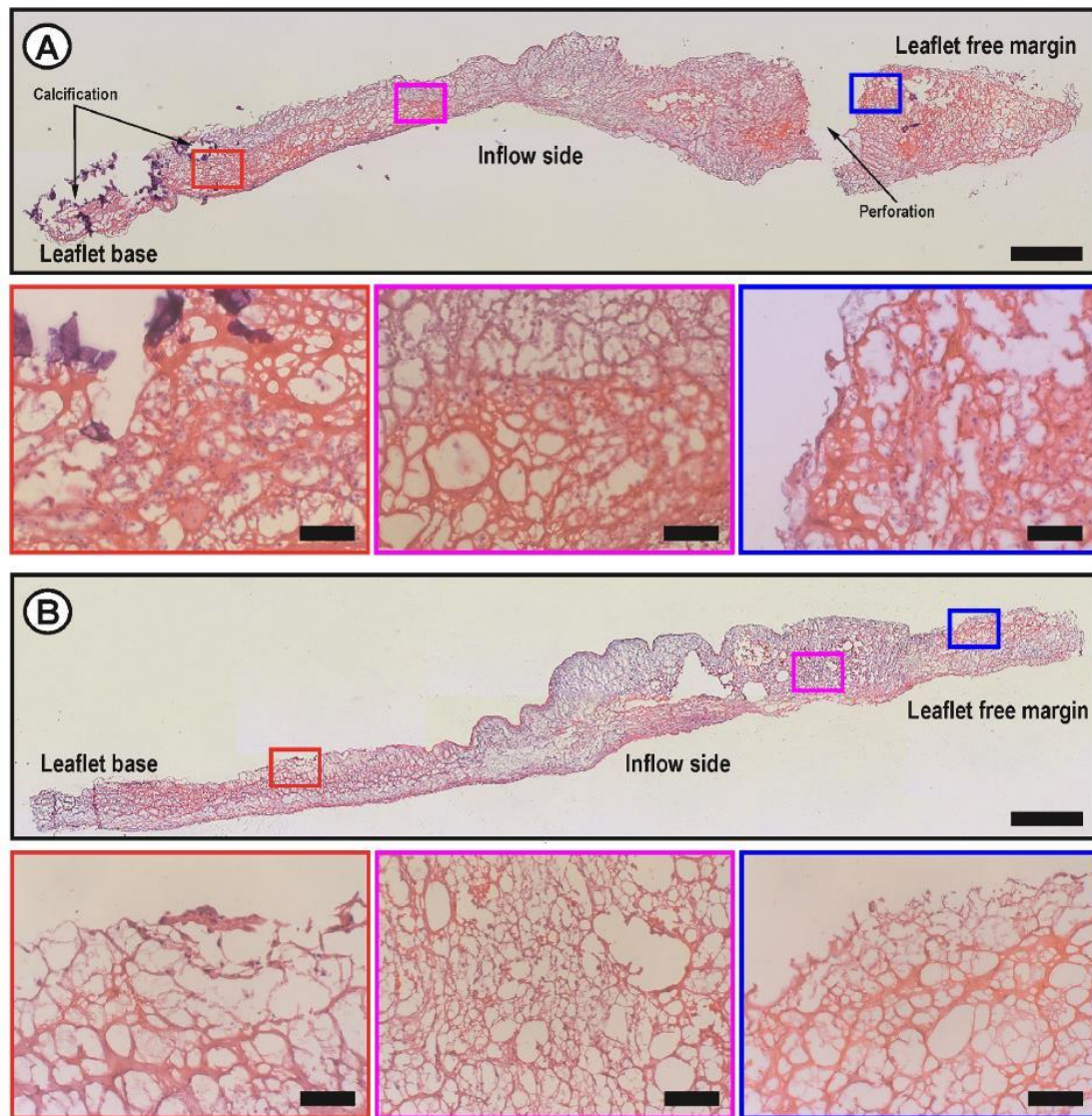


Figure S5. XAP-BHVs are prone to cellular infiltration. **A.** Moderate cellular infiltration. Note the absence of host cells in the deep ECM layers and numerous cells at the leaflet surface or underneath. **B.** Aggressive cellular infiltration was restricted to the leaflets with calcium deposits and perforations, having been associated with these lesions. For A and B: images at the bottom are close-ups of those at the top (demarcated by red, purple, or blue contour). Haematoxylin and eosin staining, representative images, magnification: x50 (overview, merged image) and x200 (close-ups), scale bars: 1000 μm (overview, merged image) and 100 μm (close-ups). XAP-BHVs – xenoaortic porcine bioprosthetic heart valves, ECM – extracellular matrix.

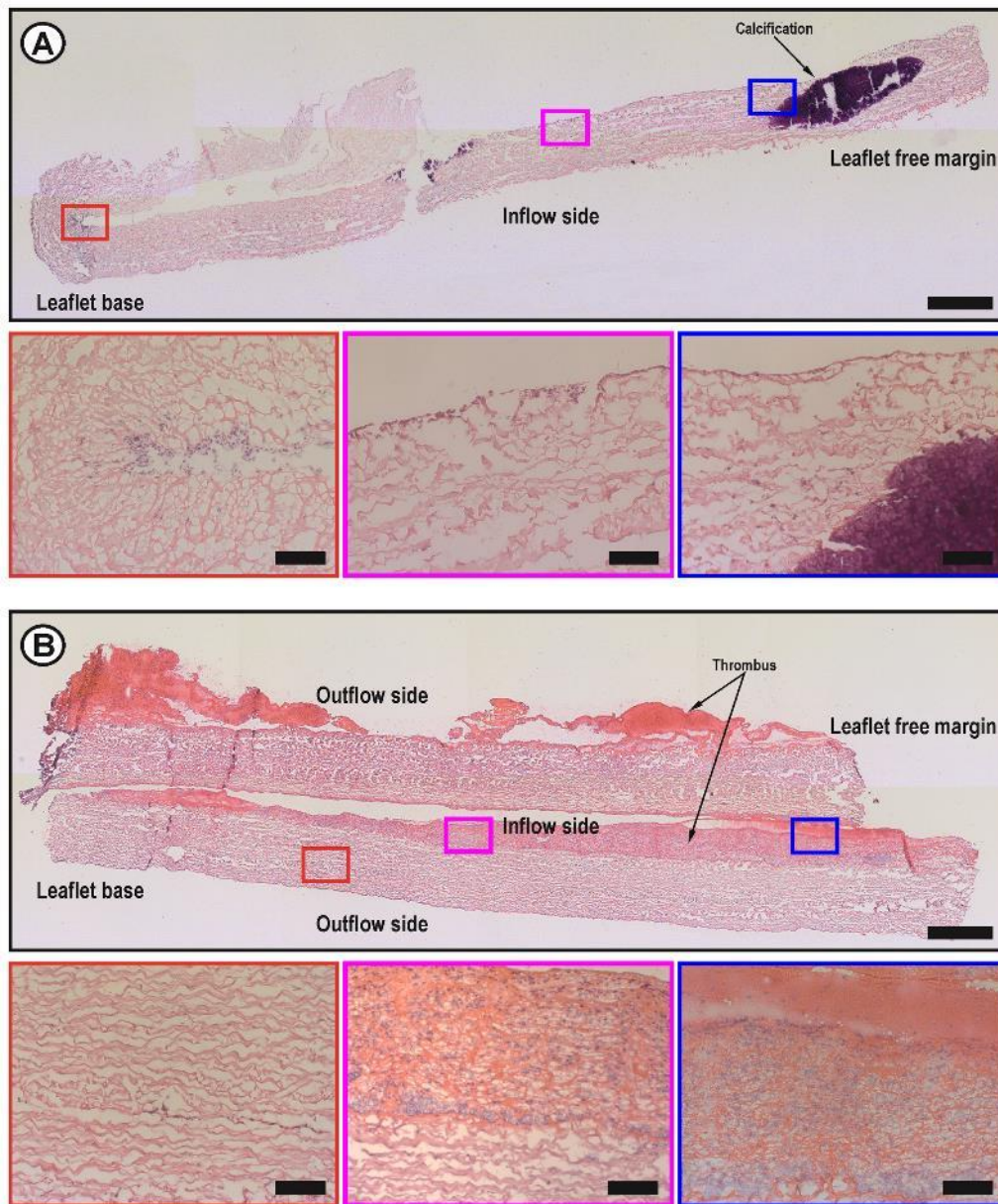


Figure S6. XPB-BHVs display weak cellular infiltration. **A.** Almost all leaflets contained minor amounts of host cells at the surface or underneath. **B.** Leaflets of the BHV which failed because of thrombosis 2 days postimplantation did not contain any cells. Yet, thrombotic masses were heavily populated by neutrophils. For A and B: images at the bottom are close-ups of those at the top (demarcated by red, purple, or blue contour). Haematoxylin and eosin staining, representative images, magnification: x50 (overview, merged image) and x200 (close-ups), scale bars: 1000 μm (overview, merged image) and 100 μm (close-ups). XPB-BHVs – xenopericardial bovine bioprosthetic heart valves.

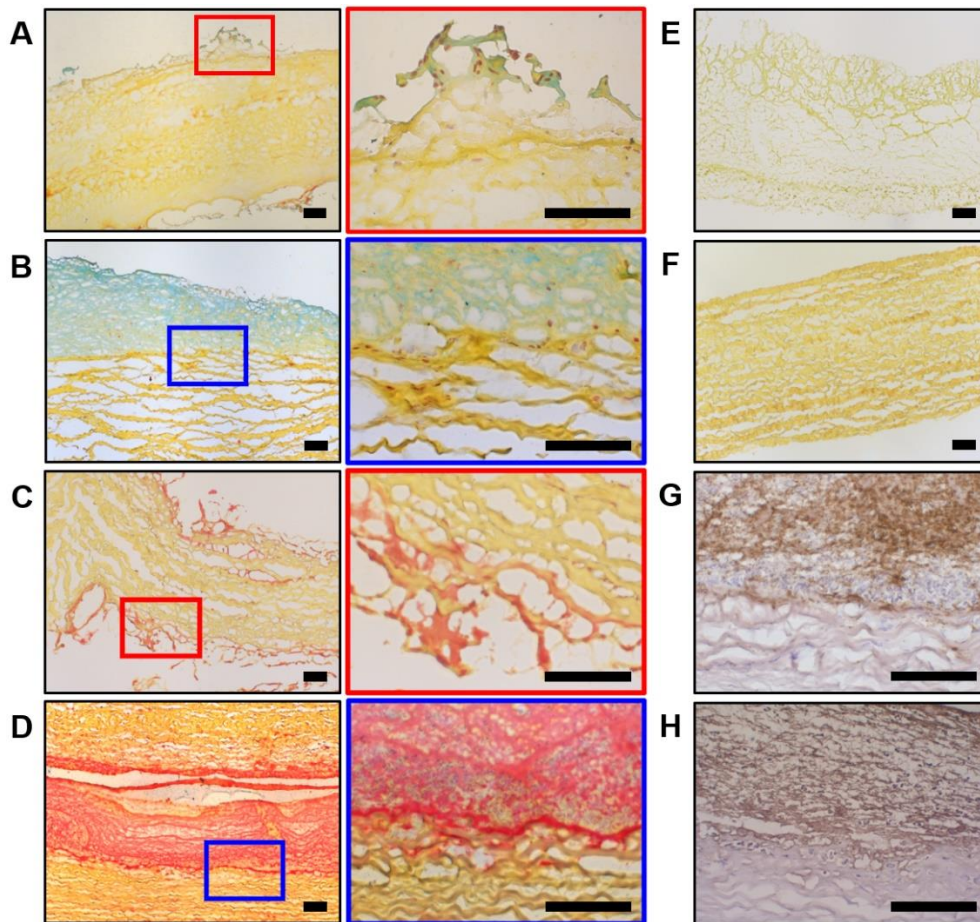


Figure S7. Russell-Movat's pentachrome staining delineates the basic components of the bioprosthetic ECM. A. Prosthetic ECM within the XAP-BHVs and XPB-BHVs consisted of collagen (yellow colour) while invading host cells produced notable amounts of glycosaminoglycans (turquoise colour). **B.** Abnormal connective tissue at the BHV surface (pannus) was composed of glycosaminoglycans (blue colour) and collagen (yellow colour). **C.** Fibrin (red colour) at the surface of prosthetic collagen-rich ECM (yellow colour). **D.** Prosthetic thrombus at the surface of BHV which was excised 2 days postimplantation because of immunothrombosis (positive control for fibrin staining). For A–D: images to the right are close-ups of those to the left (demarcated by red or blue contour). Russell-Movat's pentachrome staining, magnification: x100 (left) and x400 (right). **E.** Non-implanted XAP-BHV was solely composed of collagen. **F.** Non-implanted XPB-BHV also consisted exclusively of collagen. For E and F: Russell-Movat's pentachrome staining, magnification: x100. **G.** CD41 staining (brown

colour) of the BHV excised 2 days postimplantation because of immunothrombosis (positive control for platelets, i.e., for thrombosis). **H.** Fibrin staining (brown colour) of the BHV excised 2 days postimplantation because of immunothrombosis (positive control for fibrin). For G and H: immunohistochemical staining, magnification: x400. For A–H: representative images, scale bars: 100 μm . ECM – extracellular matrix, XAP-BHVs – xenoaortic porcine bioprosthetic heart valves, XPB-BHVs – xenopericardial bovine bioprosthetic heart valves, ECM – extracellular matrix, CD – cluster of differentiation.

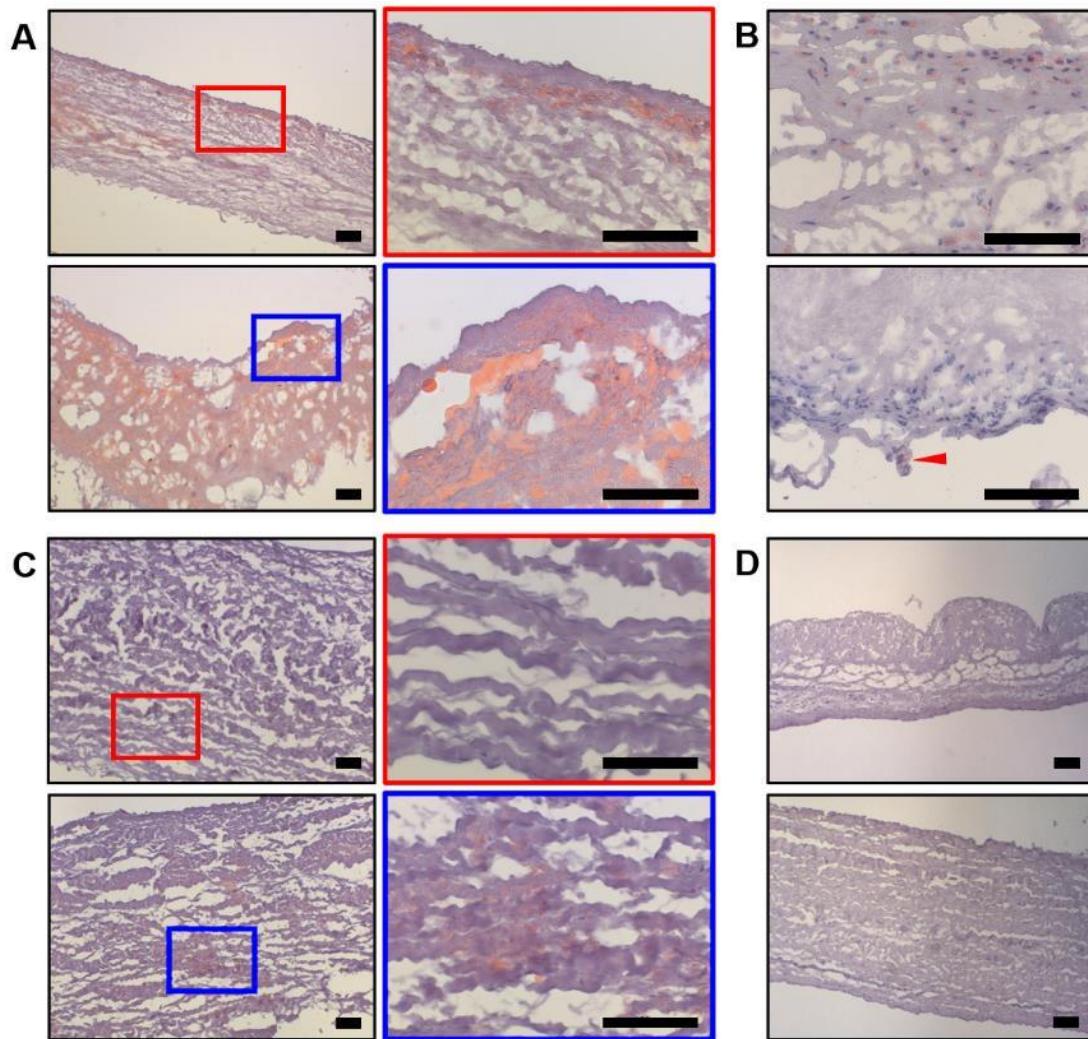


Figure S8. Patterns of lipid deposition in XAP-BHVs and XPB-BHVs. **A.** Fatty streaks (top) and fatty spots (bottom) characteristic for XAP-BHVs. Images to the right are close-ups of those to the left (demarcated by red or blue contour). Magnification: x100 (left) and x400 (right). **B.** Foam cells (i.e., macrophages which engulfed lipid droplets) abundantly detected in XAP-BHVs. Magnification: x400. **C.** 4 out of 5 XPB-BHVs did not contain lipids (top) whereas the remaining one had medium amount of lipid droplets within the leaflets (bottom). Images to the right are close-ups of those to the left (demarcated by red or blue contour). Magnification: x100 (left) and x400 (right). **D.** Absence of lipids in XAP-BHV (top) and XPB-BHV (bottom) which have not been implanted. Magnification: x100. For A–D: Oil red O staining, representative images, scale bars: 100 μm . XAP-BHVs – xenoaortic porcine bioprosthetic heart valves, XPB-BHVs – xenopericardial bovine bioprosthetic heart valves.

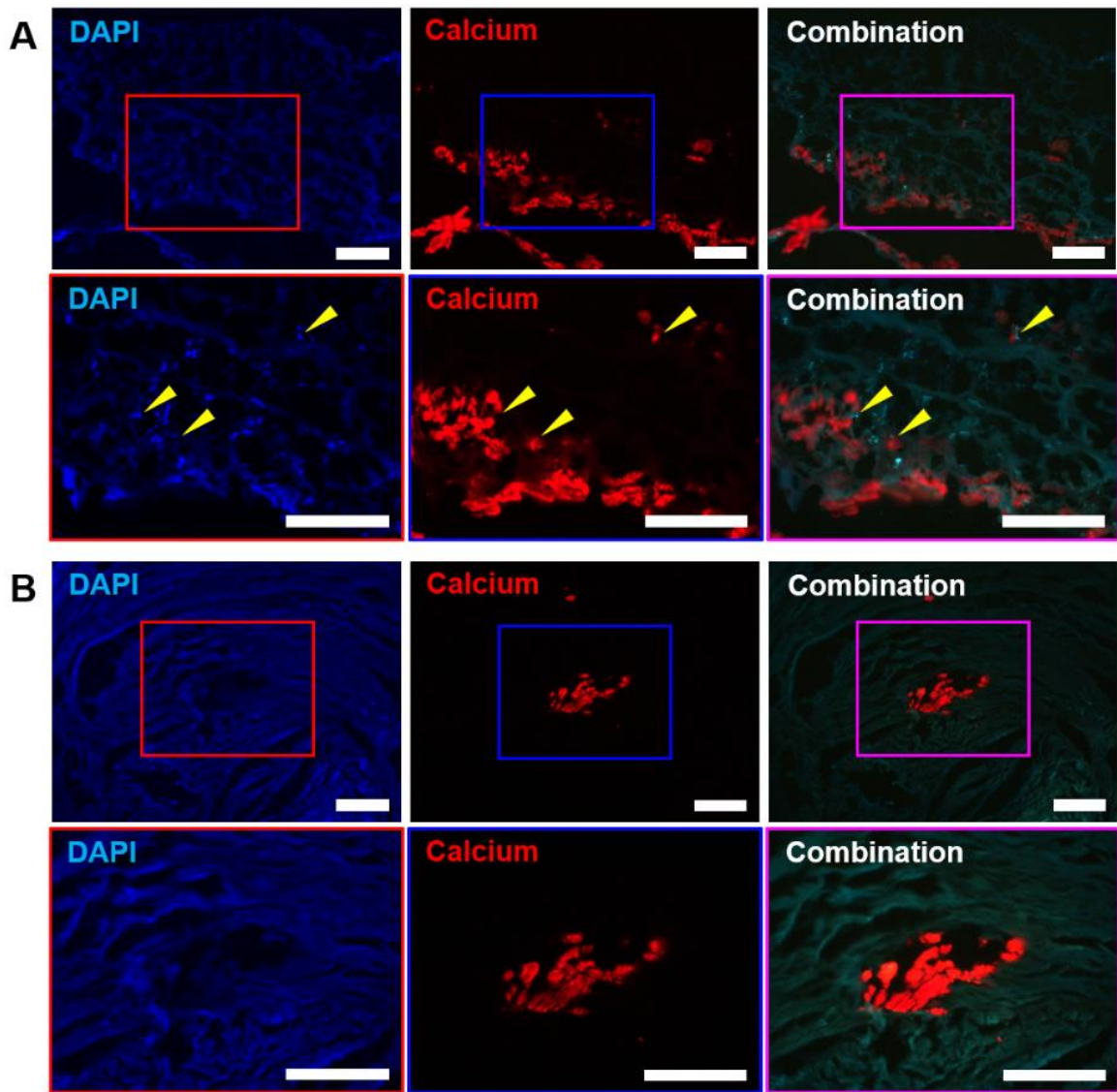


Figure S9. Patterns of calcification in XAP-BHVs and XPB-BHVs. **A.** Microcalcifications (red colour) co-localised with the host cells (indicated by yellow arrows) suggestive of passive deposition of Ca^{2+} ions on the cell debris. **B.** Mineral deposits (red colour) in the ECM devoid of cells also provide evidence for the dystrophic calcification of the degraded ECM components. For A and B: images at the bottom are close-ups of those at the top (demarcated by red, blue, or purple contour). Alizarin red S staining (red colour) combined with nuclear counterstaining (DAPI, blue colour), representative images, magnification: x200 (top) and x400 (bottom), scale bars: 100 μm . XAP-BHVs – xenoaortic porcine bioprosthetic heart valves, XPB-BHVs – xenopericardial bovine bioprosthetic heart valves, ECM – extracellular matrix, DAPI – 4',6-diamidino-2-phenylindole.